Journal of Structural Geology 163 (2022) 104705

Contents lists available at ScienceDirect

Journal of Structural Geology

journal homepage: www.elsevier.com/locate/jsg

Compiling regional structures in geological databases: The giant quartz veins of the Pyrenees as a case study

Eloi González-Esvertit [a,*], Àngels Canals [a], Paul D. Bons [b,c], Josep Maria Casas [d], Enrique Gomez-Rivas [a]

[a] Departament de Mineralogia, Petrologia i Geologia Aplicada, Facultat de Ciències de la Terra, Universitat de Barcelona. C/Martí i Franquès s/n, Barcelona, 08028, Spain
[b] Department of Geosciences, Tübingen University, Schnarrenbergstrasse 94-96, 72076, Tübingen, Germany
[c] China University of Geosciences, Beijing, China
[d] Departament de Dinàmica de la Terra i l'Oceà, Facultat de Ciències de la Terra, Universitat de Barcelona. C/Martí i Franquès s/n, Barcelona, 08028, Spain

ARTICLE INFO

Keywords:
Database
Geological structures
Giant quartz veins
Pyrenees

ABSTRACT

Gathering and arranging specific data related to different types of geological structures in thematic and interactive databases has become central for the geosciences. However, a well-defined workflow to achieve this goal is currently lacking. We present a Geographical Information System-based method for the systematic compilation, evaluation, and interpretation of regional geological structures. The method is demonstrated by indexing 741 giant quartz veins cropping out along the Pyrenees (SW Europe) in a database called GIVEPY (GIant quartz VEins of the PYrenees). The GIVEPY database incorporates information of the geometry, distribution, and statistics of the indexed veins, as well as of their host rocks, and can serve as a starting point for boosting the understanding of giant quartz veins in the Pyrenees and other areas. The first-order structural controls on vein emplacement are hypothesized on the basis of vein distribution and linkage with other brittle and ductile structures, such as faults, folds, shear zones, and regional foliations. Furthermore, we discuss the strengths and limitations of the workflow and its potential application to other geological structures. The GIVEPY database is dynamic and freely available at https://givepy.info/.

1. Introduction

Surface and sub-surface geological structures are common subjects of study in both academic and industry research. For instance, regional folds, faults, and shear zones are useful for constraining the evolution of sedimentary basins and orogens worldwide (*e.g.*, Fossen and Cavalcante, 2017; Nabavi and Fossen, 2021) and, together with igneous intrusions, diagenetic alterations, veins, and unconformities, are of special interest to the mining sector (*e.g.*, Candela and Piccoli, 2005; Sillitoe, 2010; Chauvet, 2019). As a result, vast amounts of surface and sub-surface data of different types of geological structures have been generated by earth scientists, geological surveys, and mining and hydrocarbon exploration companies for centuries. The progressive adoption of open access data policies by funding agencies, institutions, and research communities makes these data potentially reusable for further research and applications (*e.g.*, Stall et al., 2019; Chamberlain et al., 2021).

Inventorying distinct types of geological structures and organizing their information in thematic and interactive databases can significantly contribute to the growth of geoscience knowledge, including that in structural geology and tectonics. However, data are commonly scattered in different reports, maps, and databases, and no well-defined and standard workflows for gathering geological structures are available. Here we present a workflow within a Geographic Information System (GIS) environment to systematically compile and organize information to characterise geological structures. The method is applied to the indexation of large quartz veins cropping out in the Pyrenean fold and thrust belt (SW Europe). It is proposed that the same workflow and approach can potentially be applied to other geological structures and replicated in other tectonic settings.

Quartz veins are ubiquitous in orogenic belts, especially along zones of localized deformation such as faults and fractures in the upper (brittle) crust and shear zones in the lower (ductile) crust (Bons, 2000; Bons et al., 2012; Lemarchand et al., 2012). Classically, quartz veins have been considered as valuable tools to gain understanding of fluid

* Corresponding author.
E-mail address: e.gonzalez-esvertit@ub.edu (E. González-Esvertit).

https://doi.org/10.1016/j.jsg.2022.104705
Received 29 December 2021; Received in revised form 25 July 2022; Accepted 14 August 2022
Available online 24 August 2022
0191-8141/

flow mechanisms, vein cement precipitation and quartz deformation, as well as to unravel paleo-stress fields, deformation kinematics and the geochemical history of their host rocks (Cox, 1987; Fisher and Brantley, 1992; Sharp et al., 2005; Bons et al., 2012; Fagereng et al., 2018). Furthermore, quartz veins are often intimately related with different types of ore mineralization, *e.g.*, in orogenic gold (Zhang et al., 2020), porphyry-type (Müller et al., 2010), and epithermal (Dong et al., 1995) ore deposits. The dimensions of quartz veins (such as their length and width) can vary dramatically within the same tectonic setting, with thicknesses ranging from millimetres to tens or even hundreds of metres

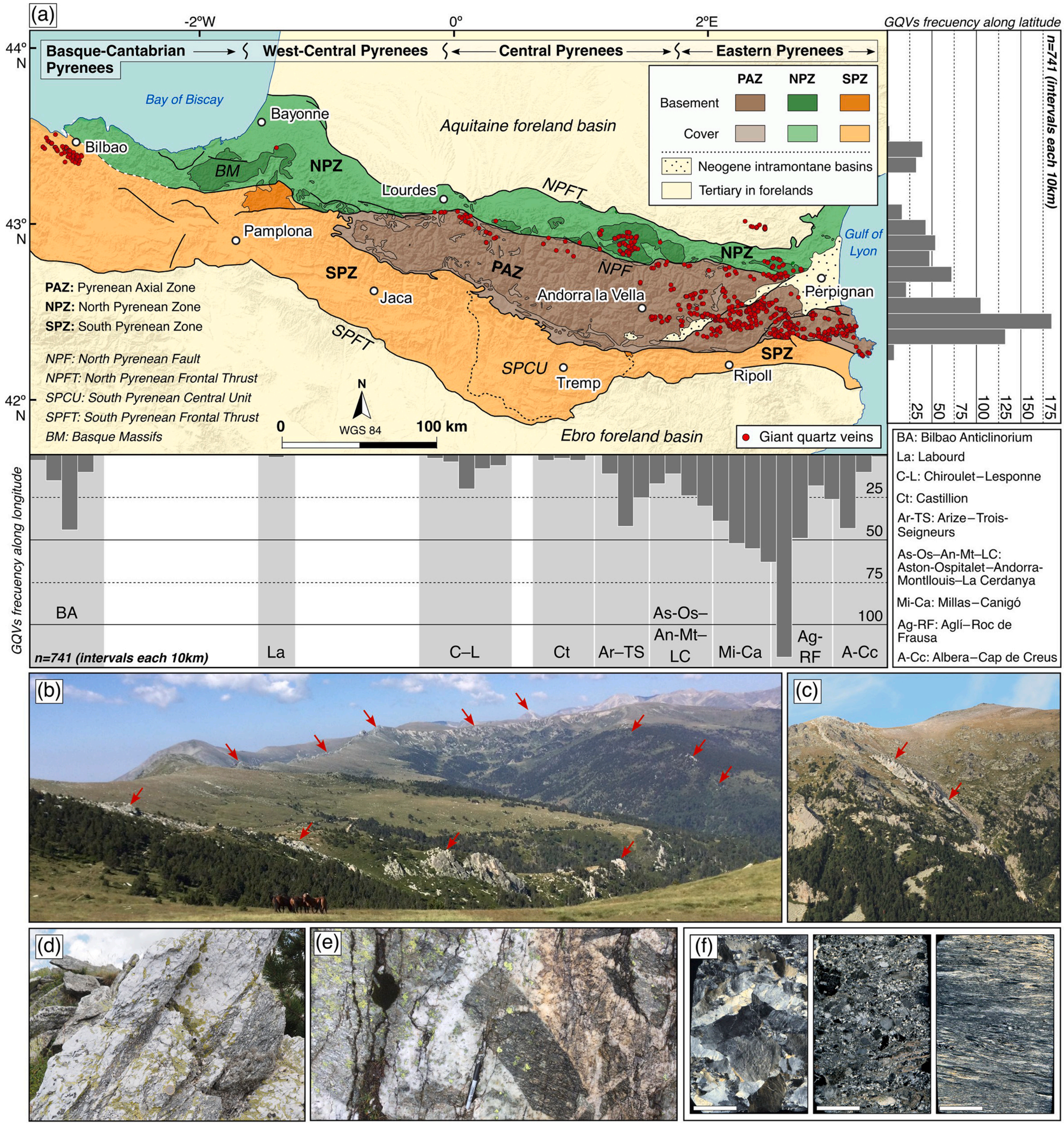

Fig. 1. (a) Distribution of the Giant Quartz Veins (GQVs) of the Pyrenees at the orogen scale. Histograms showing the frequency (n) of veins along the longitude (bottom side) and latitude (right side) of the chain. E-W sub-divisions are taken from Miró et al. (2020) and Muñoz (2002), and N–S sub-divisions from IGME-BRGM (2009). (b) Example of the GQVs of the Canigó Massif (red arrows); four horses for scale. (c) Landscape view of a lens shaped GQV from the Canigó Massif (red arrows), ca. 10 km southwards the Gra de Fajol summit. (d, e) Representative outcrops of the GQVs of the Pyrenees. (f) High-resolution scans of representative thin sections of the GQVs of the Canigó Massif showing, from left to right: low-grade intra-crytalline deformation in euhedral quartz crystals, brittle deformation and cataclastic flow, and ductile deformation and mylonitization (cross polarized light; scalebars are 1 cm). (For interpretation of the references to colour in this figure legend, the reader is referred to the Web version of this article.).

and with lengths spanning centimetres to kilometres. Those veins that are visible in satellite and photogrammetric imagery, *i.e.*, mappable at the 1:25,000 scale, are referred to in this work as “Giant” Quartz Veins (GQVs). Despite their ubiquity, their formation mechanisms remain unclear to date: it has been proposed that they can form by quartz precipitation from extremely large volumes of externally-derived fluids (Lemarchand et al., 2012; Tannock et al., 2020), although other studies have postulated that high fluid/rock ratios are not necessarily required and that, accordingly, fluid may be more locally sourced (*e.g.*, Bons, 2001; Wangen and Munz, 2004; Sharp et al., 2005; de Riese et al., 2020).

Fieldwork-based small-scale analyses of the orientation and distribution of centimetre-to metre-wide veins are common and provide key information about their formation time, mechanisms, relative stress and fluid pressures (*e.g.*,Yardley et al., 1993; André et al., 2001; Boiron et al., 2003; Kenis et al., 2005; Mondal and Mamtani, 2013; González-Esvertit et al., 2020; Lahiri et al., 2020). Because of their exceptional sizes, large veins can also be analysed using macroscale remote sensing and other computer-assisted methods (*e.g.*, Holland et al., 2009). GIS software packages provide suitable environments for these purposes, since digitised traces of GQVs combined with satellite imagery, high-resolution Digital Elevation Models (DEMs), and orthophotographs allow determining or estimating their orientation, distribution, associated structures, and host rock(s), thus gaining new insights into the structural controls on large vein emplacement.

The Pyrenees represents an excellent natural laboratory for this purpose due to the existence of large, open access, and regularly updated datasets provided by the Spanish, Catalan, Andorran and French geological surveys. Hundreds of GQVs are hosted by different rocks in the Pyrenees (Fig. 1), although they have only been the subject of a few studies: those by Ayora and Casas (1983) and Casas (1986) in the Canigó Massif (Esquerdes de Rojà; Fig. 1b–f) and that by Fonseca et al. (2015) in the Cap de Creus Massif (Roses area). The age of these structures is under discussion: most of the GQVs have classically been attributed to the Variscan Orogeny (ca 330 to 290 Ma), but in the southern and northern slopes of the Pyrenean chain, some GQVs are also hosted in Jurassic, Cretaceous and Eocene sedimentary rocks, thus being post-Variscan in age. In fact, the only dating carried out on a GQV from the Pyrenees yield an Alpine age (Espínola et al., 1997).

In this contribution open access datasets are mined and curated to obtain the main features of 741 GQVs and their host rocks. The dataset is presented as a dynamic and interactive database called GIVEPY (GIant quartz VEins of the PYrenees), which follows the FAIR principles of database management (Findable, Accessible, Interoperable and Reusable; Wilkinson et al., 2016). This product allows carrying out a statistical-geometrical analyses of GQVs attributes, including their dimensions (lengths and width), orientation and distribution along the Pyrenean chain, as well as to discussing their relationship with other tectonic structures previously highlighted in the literature (shear zones, fractures, folds, and faults). The GIVEPY database aims to be a useful resource for academic research, acting as a “targeting tool” for location choice before carrying out studies on GQVs, their host rocks or their related (macro to micro) structures. Furthermore, the GIVEPY database can also be used for structural geology and tectonics teaching, as it provides examples and information of exceptional outcrops of large quartz veins.

2. Geological setting

2.1. The Pyrenees

The Pyrenean chain is an Alpine fold-and thrust belt formed from the late Cretaceous to the Miocene by the collision between the Iberian and Eurasian plates (Muñoz, 1992). In the central part of the chain, Alpine thrusts formed an antiformal stack that resulted in the exhumation of the pre-Variscan basement rocks (Muñoz, 1992). Pre-Variscan basement is mainly composed of a late Neoproterozoic–to–Carboniferous metasedimentary succession, Variscan gneisses derived from late Neoproterozoic and Ordovician intrusives, and late-Variscan granitoids (Fig. 2) (Santanach, 1972a, 1972b; Muñoz, 1992; Casas, 2010; Pereira et al., 2014; Navidad et al., 2018; Padel et al., 2018b). These rocks provide evidence of late Neoproterozoic (Cadomian), Ordovician (Sardic) and Carboniferous (Variscan) episodes of igneous activity (Cocherie et al., 2005; Liesa et al., 2008; Casas et al., 2010, 2015; Pereira et al., 2014; Martínez et al., 2016; Navidad et al., 2018; Padel et al., 2018a), as well as Ordovician, Variscan and Alpine deformation events (Guitard, 1970; Zwart, 1986; Muñoz, 1992; Casas, 2010). The North Pyrenean (NPZ) and South Pyrenean (SPZ) Zones on either side of the Pyrenean chain represent foreland-directed fold-and-thrust belts towards the northern Aquitanian basin and southern Ebro basin, respectively (Fig. 1). The NPZ is broadly composed of a strongly folded Jurassic to Lower Cretaceous carbonate platform and an Upper Cretaceous turbiditic flysch succession, with north-verging thrust imbricates that have been detached above Upper Triassic evaporites (Canérot et al., 2005; Ford et al., 2016; Ford and Vergés, 2021). Mantle rocks exhumed during the Cretaceous hyper-extension, as well as metamorphic rocks formed during the Upper Cretaceous HT-LP contact metamorphism are also present along the southern sector of the NPZ (Tugend et al., 2015; Lagabrielle et al., 2016, 2020). In the SPZ, internal Alpine overthrusts between the Mesozoic and Cenozoic rocks define three main thrust sheets which were detached over the Upper Triassic evaporites and displaced further southwards above the Eocene evaporites (*e.g.*, Muñoz et al., 2013, 2018; Santolaria et al., 2017) (Fig. 1).

2.2. Giant quartz veins

Hundreds of quartz veins with lengths of hundreds of metres to kilometres are found throughout the Pyrenees (Figs. 1 and 2). They are mostly present in the pre-Alpine basement rocks (Fig. 2), although some GQVs are also hosted in the sedimentary rocks of the SPZ and (more often) the NPZ (see the geological maps listed in Table 1). They often record proto-cataclastic to ultramylonitic deformation (Fig. 1d, f), which could either have been developed after their emplacement or been inherited from the host rock structure during vein-forming silicification processes (Ayora et al., 1984). Their emplacement has been inferred to be controlled by regional structural features such as mylonitic bands, faults, and shear zones of different age and origin (*i.e.*, Carreras and Losantos, 1982; Liesa, 1988; Le Bayon and Cochelin, 2020; González-Esvertit et al., 2022, and the geological maps listed in Table 1). Phyllosilicates and/or calcite are present in minor amounts, and often the main quartz bodies are crosscut by anastomosing centimetre-width quartz veinlets that record minor deformation. Host rock fragments within the main quartz bodies and host rock silicification processes near their boundaries are also common features (Fig. 1e) (Ayora and Casas, 1983; Ayora et al., 1984; Liesa, 1988; Fonseca et al., 2015).

The GQVs of the Pyrenees are often mentioned and/or mapped in classic and more recent regional geological publications of the orogen (Guitard, 1965, 1970; Casas, 1986; McCaig et al., 1990; Espínola, 1997; Carreras et al., 2004; Laumonier, 2015; Le Bayon and Cochelin, 2020). Although a late-Variscan age has been proposed for the GQVs (see the geological maps listed in Table 1), these veins have hardly been subject of specific geochemical or structural investigations. The only absolute dating, obtained through K–Ar on K-feldspar from a GQV hosted in the Santa Coloma granodiorite (Andorra-Montlluís Massif, Eastern Pyrenees), yielded a Late Cretaceous age (81 Ma ± 3 Ma) (Espínola et al., 1997). In the Canigó Massif (Figs. 1b, c and 2), 2–15 km long and 10–25 m wide veins of massive quartz aggregates were investigated by Ayora and Casas (1983) and Casas (1984). The authors identified an E-W mylonitic and a N–S fracture systems within the main quartz bodies, although their bulk work was mainly focused on fluid inclusions thermometry. To the east of the Canigó Massif, a structural overview and a detailed fluid inclusions characterisation was carried out by Ayora et al. (1984) in three quartz bodies from the Roc de Frausa Massif and in two

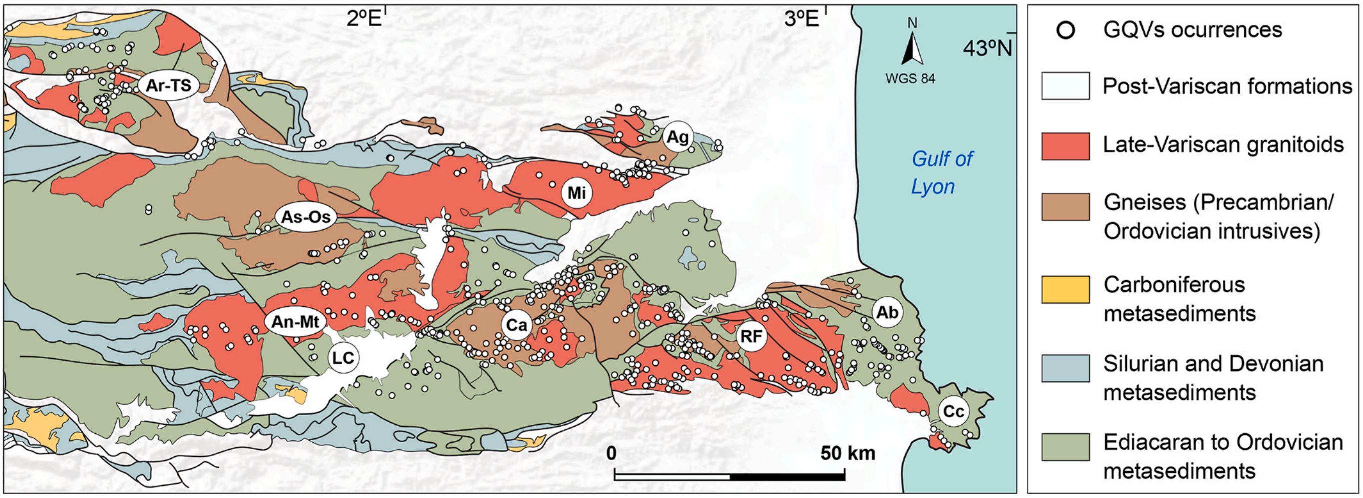

Fig. 2. Geological map of the Central-Eastern Pyrenean Axial zone with the main giant quartz vein outcropping sectors indicated; see Fig. 1 for abbreviations. Note that the veins are mostly hosted by the Palaeozoic basement of the Pyrenees, although some of them are also located within post-Variscan formations.

GQVs from the Albera and Cap de Creus massifs (see also Fonseca et al., 2015) (Fig. 2). These authors postulated that the veins emplacement occurred independently of their host rock type and was completely controlled by previous ductile structures: mylonitic bands when placed within crystalline rocks and folds affecting the regional foliation when located within metasedimentary rocks. Finally, González-Esvertit et al. (2022) suggested an Alpine age for the 300 m-long GQV of Gréixer in La Cerdanya area (southern slope of the Canigó Massif). This vein was emplaced along a gently north dipping limb of a major fold, following a south-directed Alpine thrust and registering a formation temperature of 140–180 °C, as revealed by semi-empirical chlorite thermometry (González-Esvertit et al., 2021a).

3. Methods

3.1. Data mining and database building

The proposed workflow (summarised in Fig. 3) has been devised to address individual structures with a minimum outcrop area of ca. 1000 m^2 or length of ca. 100 m (*i.e.*, mappable at the 1:25,000 scale). Thus, the following procedures can be used or adapted for the development of databases comprising geological features of similar dimensions or larger, such as faults, igneous bodies, salt diapirs, folds, or shear zones (among others).

Source layers used throughout the workflow, with their respective scale and attribution, are shown in Table 1. The Geological maps at 1:50,000 scale of IGME (Instituto Geológico y Minero de España; https://igme.es), ICGC (Institut Cartogràfic i Geològic de Catalunya; https://icgc.cat), IEA-SIGMA (Institut d'Estudis Andorrans – Sistema d'Informació Geogràfica Mediambiental d'Andorra; https://www.iea.ad/sigma), and BRGM (Bureau de Recherches Géologiques et Minières; https://brgm.fr) were used as a starting point for the GQVs macrostructural analysis (Fig. 3). Their format is in all cases a vector-based ESRI® Shapefile, and the geological units mapped within are thus represented by polygons. Topology rules were applied to all the original files to detect and fix overlaps and gaps between polygons. Two duplicated copies of each corrected layer were required to develop the GIVEPY database. The first layer duplicates were filtered by polygon attributes to only extract the shape and properties of the GQVs. Inversely, the second layer duplicates were filtered by polygon attributes to only extract the host rocks shape and properties (age, type, and description). Layer copies with GQVs information from each region (Table 1) were semi-automatically unified and merged to obtain a unique vector file where the GQVs of the Pyrenees are mapped as individual features. Otherwise, untidied data attributes and outdated names of rock types and stratigraphical units were found in the source layers corresponding to the host rock properties, especially in those regarding the Palaeozoic metasedimentary successions. Thus, host rock layer duplicates required a step-by-step manual editing to adhere to the latest stratigraphical correlations and ages of magmatism (*e.g.*, Castiñeiras et al., 2008; Vacherat et al., 2017; Navidad et al., 2018; Padel et al., 2018a, 2018b; Martí et al., 2019). Up to 500 original host rock types were manually unified though this data curation process, resulting in the Final Host Rock Layer (Fig. 3) that now contains 208 host rock types.

The mapping accuracy of GQV shapes was improved manually on the basis of two main sources (Fig. 3, Table 1): (1) remote-sensing images, including high-resolution aerial orthophotographs from PNOA-IGN (Plan Nacional de Ortofotografía Aérea - Instituto Geográfico Nacional; https://ign.es) and IGN (Institut Géographique National; https://ign.fr), and satellite images from COAH (Copernicus Open Access Hub; https://scihub.copernicus.eu/), and (2) published data and regional geological maps (*e.g.*, Guitard, 1965, 1970; Autran and Guitard, 1968; Casas, 1986; Le Bayon and Cochelin, 2020; González-Esvertit et al., 2022). Furthermore, LiDAR-derived high-resolution DEMs provided by ICGC were used as cost rasters through a least-cost path approach to perform (when possible) a semi-automatic (supervised) mapping of GQVs from the Eastern Pyrenees, using the plugin GeoTrace (Thiele et al., 2017). This allowed the automated improvement of the trace of GQVs when DEM resolution and veins relief are high enough so that veins appear as topographic ridges.

After the GQV shape correction, geometry calculations were applied to the GQV features to derive their outcrop area, UTM coordinates, and mean azimuth, stored in the GQV Final Layer (Fig. 3). The attributes in the GQV and the Host Rock Final Layers were joined by location to derive the GIVEPY database, where the GQVs of the Pyrenees are indexed as spatial features. Each of them includes, as individual attributes, the geological and geospatial information of their geometry, host rocks (*i.e.*, lithology, age, and rock type), and regional geological setting (*i.e.*, the Pyrenean units or domains where they crop out) (Fig. 3).

3.2. Data curation and analysis

The GIVEPY database has allowed the analysis of the GQVs of the Pyrenees through three different approaches (Fig. 3): (1) an overall assessment of their location and host rock types (Sub-section 4.2), (2) a statistical-geometrical analysis of their morphology and orientation according to their location and host rock variability (Sub-section 4.3), and

Table 1
Source layers used as starting point for the GIVEPY database building process with their corresponding reference.

Layer name	Scale/ Resolution	Zone	Usage	Referenced source
Vector:				
IGME-GEODE	1:50,000	West-Central and Basque-Cantabrian Pyrenees (Spain)	Geology (Source)	Instituto Geológico y Minero de España, IGME. Mapa Geológico Continuo de España. Available at: http://igme.es/
IEA-SIGMA	1:25,000	Andorra	Geology (Source)	Institut d'Estudis Andorrans, Centre d'Estudis de la Neu i la Muntanya d'Andorra, IEA-CENMA. Servei d'Informació Geogràfica i Mediambiental d'Andorra (SIGMA). Available at: https://iea.ad.
BRGM-D09	1:50,000	Département de l'Ariège (France)	Geology (Source)	Bureau de Recherches Geologiques et Minaires, BRGM. Cartes géologiques vectorisées et harmonisées, Département 09, available at https://brgm.fr
BRGM-D11	1:50,000	Département de l'Aude (France)	Geology (Source)	Bureau de Recherches Geologiques et Minaires, BRGM. Cartes géologiques vectorisées et harmonisées, Département 11, available at https://brgm.fr
BRGM-D31	1:50,000	Département de la Haute-Garonne (France)	Geology (Source)	Bureau de Recherches Geologiques et Minaires, BRGM. Cartes géologiques vectorisées et harmonisées, Département 31, available at https://brgm.fr
BRGM-D64	1:50,000	Département des Pyrénées-Atlantiques (France)	Geology (Source)	Bureau de Recherches Geologiques et Minaires, BRGM. Cartes géologiques vectorisées et harmonisées, Département 64, available at https://brgm.fr
BRGM-D65	1:50,000	Département des Hautes Pyrénées (France)	Geology (Source)	Bureau de Recherches Geologiques et Minaires, BRGM. Cartes géologiques vectorisées et harmonisées, Département 65, available at https://brgm.fr
BRGM-D66	1:50,000	Département des Pyrénées-Orientales (France)	Geology (Source)	Bureau de Recherches Geologiques et Minaires, BRGM. Cartes géologiques vectorisées et harmonisées, Département 66, available at https://brgm.fr
ICGC-MGC	1:50,000	Central and Eastern Pyrenees (Spain)	Geology (Source)	Institut Cartogràfic i Geològic de Catalunya, ICGC. Mapa geològic comarcal 1:50,000, available at https://icgc.cat
ICGC-GT-I	1:25,000	Central and Eastern Pyrenees (Spain)	Geology (Source)	Institut Cartogràfic i Geològic de Catalunya, ICGC. Mapa geològic GT I 1:25,000 (sheets 77-20-Agullana; 78-20-Garriguella; 78-21-Castelló d'Empúries and 79-21-Roses), available at https://icgc.cat
Raster				
Published geological maps	See references	Roc de Frausa/Canigó/La Cerdanya	Mapping improvement	Autran and Guitard (1968); Casas (1986); González-Esvertit et al. (2022); Guitard (1970, 1965); Le Bayon and Cochelin (2020)
ICGC-HR-DEM	2 × 2 m (LiDAR)	Central and Eastern Pyrenees (Spain)	Mapping improvement	Institut Cartografic i Geologic de Catalunya, ICGC. Model d'Elevacions del Terreny de Catalunya 2 × 2metres (MET-2) v1.0, available at https://icgc.cat
ICGC-OP	25 cm	Central and Eastern Pyrenees (Spain)	Mapping improvement	Institut Cartografic i Geologic de Catalunya, ICGC. Ortofoto de Catalunya 25 cm v4r0, available at https://icgc.cat
PNOA-IGN	25 cm	West-Central and Basque-Cantabrian Pyrenees (Spain)	Mapping improvement	Plan Nacional de Ortofotografía Aérea del Instituto Geográfico Nacional, PNOA-IGN. Ortofotografías aéreas digitales con resolución de 25 cm. Available at: https://pnoa.ign.es/
IGN-OP	50 cm	Central and Eastern Pyrenees (France)	Mapping improvement	Institut National de l'Information Géographique et Forestière, IGN. Photographies Aériennes Dématérialisées du Territoire Français à une résolution de 25 cm. Available at: https://www.geoportail.gouv.fr/donnees/photographies-aeriennes
COAH	~10 m	Specific veins	Geology (Starting point)	Copernicus Open Access Hub – European Space Agency, COAH-ESA. SENTINEL-2, ESA's Optical High-Resolution Mission for GMES Operational Services (ESA) (2020–2021). Available at: https://scihub.copernicus.eu/

(3) an evaluation of the GQV geographical and geological distribution and their potential relationship with other geological structures (Sub-section 4.4).

Prior to the statistical-geometrical analysis, the original GQV polygons were converted to equivalent polylines in order to consider each vein as a fracture trace instead of as an outcropping area (Fig. 4). This conversion was carried out by calculating the centreline of each GQV, which preserves the unaltered length, orientation, and geometry of the original polygon. Among other procedures for generating polygon centrelines from raster (*e.g.*, Hasthorpe and Mount, 2007; Pavelsky and Smith, 2008) or vector (*e.g.*, Lee, 1982; Haunert and Sester, 2004) data sources, we opted for the Voronoi Diagram method (Fig. 4), also known as Voronoi Tessellation or Thiessen algorithm (*e.g.*, Dey and Zhao, 2002). This method is one of the most standardized procedures to generate polygon centrelines. It can be applied with diverse programming languages (*e.g.*, MATLAB, C++ or Phyton, among others) and within most GIS environments. By applying this algorithm, each polygon is skeletonized by segment partitioning from each node (Fig. 4a), resulting in a complex network of skeletal trace lines among which is the polygon centreline (Fig. 4b). Peripheral trace lines and other line segments should thus be removed by filtering attributes (Fig. 4c), preserving only the final centreline of each polygon (Fig. 4d). The obtained Centrelines Layer (Supplementary Material 1) thus preserves all the attributes of the GIVEPY database and is considered as an accurate geometrical (lineal) simplification of the GQV polygons (Fig. 3).

For GQV width calculations, centreline nodes were densified by intervals to achieve regularly placed extra vertices within each segment (Fig. 5a, b). A distance of 20 m between the extra vertices was chosen to ensure a good resolution of GQV width variations in a reasonable computational time. Afterwards, 120 m-long transects oriented 90° from the centreline's direction were calculated at each node (Fig. 5c). This length value was established on the basis of the maximum GQV width to ensure that all the transects overlap entirely with the GQV polygons. Transects were clipped to the extension of their corresponding GQV polygon and their final length was calculated to obtain consecutive along-strike width measurements of each vein, every 20 m (Fig. 5d). The number of width measurements for each vein thus depends on the vein length. The resulting dataset (see Data availability section) includes 19,202 width measurements, classified according to the Vein ID# to which they correspond, and including the sampling point (*i.e.*, distance from the GQV termination). These values were used to specifically address the individual vein width variations in the statistical-geometrical analysis, whilst for the overall evaluation of the vein location, geometry, and length:width ratios (see Sub-section 4.1), the mean width values and their corresponding standard deviation from each vein were considered.

The statistical-geometrical analysis of vein strikes was carried out using the Centrelines Layer through the FracPaQ toolbox integrated in MATLAB™ (Healy et al., 2017). This software uses operations in coordinate geometry for quantifying the lengths and orientations of linear features. For their analysis, GQV centrelines were exported to ASCII files in differentiated datasets, aiming to assess their geometrical features as a

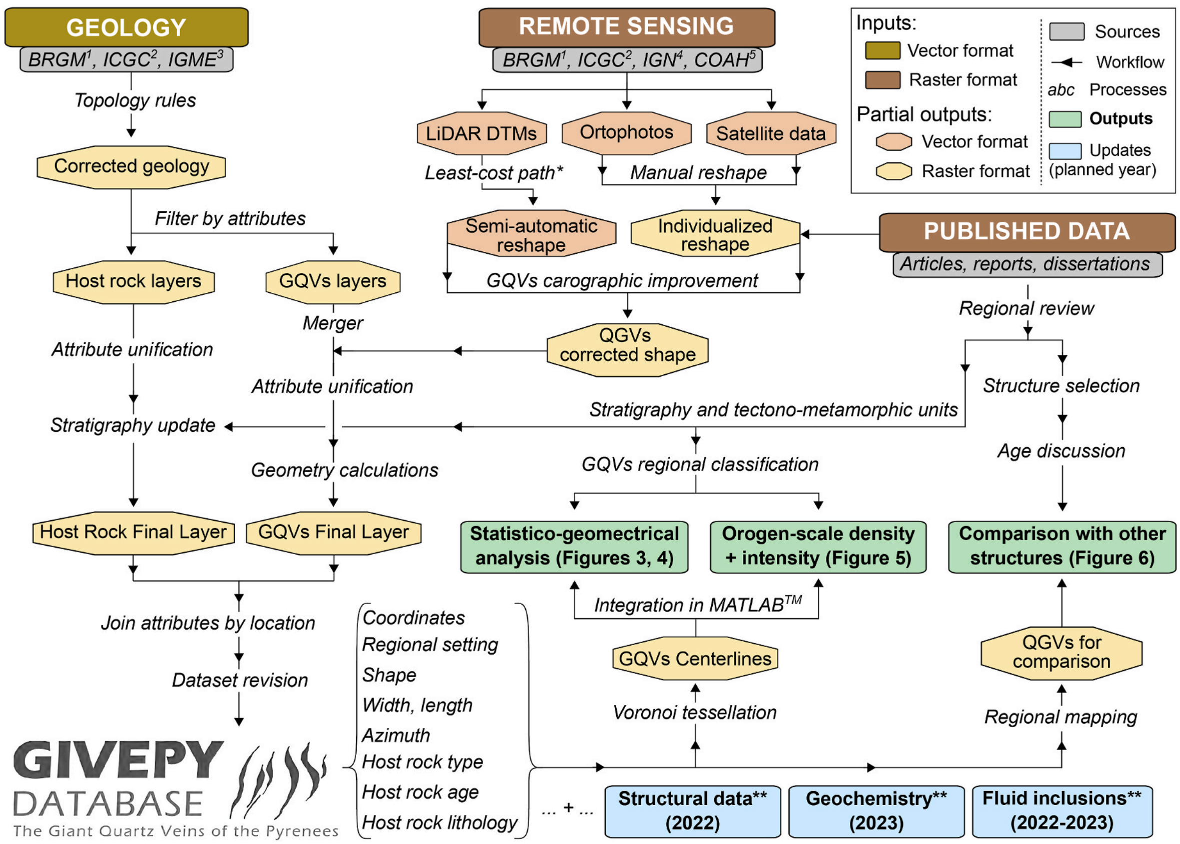

Fig. 3. Schematic workflow of the GIVEPY database building process, including the outputs presented in this work and potential future updates. [1] Bureau de Recherches Géologiques et Minières (https://brgm.fr); [2] Institut Cartogràfic i Geològic de Catalunya (https://icgc.cat); 3 Instituto Geológico y Minero de España (https://igme.es); 4 Instituto Geográfico Nacional (https://ign.es); 5 Copernicus Open Access Hub (https://scihub.copernicus.eu/); *Through the plugin GeoTrace (Thiele et al., 2017) (only applied to the GQVs that fulfil the requirements, see text for further explanations).

function of their host rocks and location. Through a specific internal data structure (Healy et al., 2017), GQV centrelines are segmented and their along-strike variations can be considered for statistical-geometric analysis. In most cases, this involves more data to analyse and, therefore, better precision of the results than considering a single linear trace that solely connects the endpoints of each GQV.

The FracPaQ code also allows analysing the intensity and density of linear features within a two-dimensional environment through the circular scan window method of Mauldon et al. (2001). The density (*i.e.*, the number of fractures per unit area) of the GQVs was addressed to obtain the distribution patterns along the chain. By this method, FracPaQ generates a 2D grid composed of a given number of spaced circular scan windows, calculates the centreline intersections and terminations within each circle, and contours each scan window according to its value using the standard MATLAB™ triangulation function. Given the (large) scale of work (*i.e.*, ~34,000 km^2), the number of scan circles has been set to 120 in order to obtain a good resolution in a reasonable computational time, either when addressing the whole dataset or the specific GQVs outcrop sectors (see Sub-section 4.4). The orogen-scale *.csv* file that contains all the GQVs of the Pyrenees is available in Supplementary Material 2. For more information regarding the FracPaQ processing methods the reader is referred to Healy et al. (2017) and the official webpage of the source code (https://fracpaq.com/).

Finally, the structural relationships and orientation similarities between some GQVs and faults, fractures, shear zones or fold axes close to them were analysed by reviewing published and unpublished geological maps, geochronological data, and other regional interpretations from the literature (Fig. 3, Table 1).

4. Results

4.1. The GIVEPY database

A total amount of 741 GQVs are indexed in the GIVEPY database as polygon-type features (see Data Availability section). Associated with each feature are 22 attributes that store additional information about their geological and geographical setting, outcropping geometry (area, width, length, and azimuth), centroid and endpoint coordinates, host rock/s (age, type, and lithology). and original source layers. Among the GQVs included in the GIVEPY database, 280 are hosted by two or more (up to eight) different host rock types. Thus, the database is built following polygon superposition rules: when a GQV has *n* types of host rocks, *n* superposed polygons with identical shape and location but different attributes regarding the host rock descriptions are included and linked to the vein that they represent through the unique vein ID#. As a result, 1,192 records (*i.e.*, features included defined by individual polygons) that represent the assessed GQVs are included in the GIVEPY database. The superposed polygons were considered for the statistical analysis of host rock types, whilst unique polygons (one per vein, independently of the number of host rock types) were used for the analysis of GQVs morphology and orientation.

The building process and format of the datasets will allow periodic updates of the GIVEPY database as more and new data become available (Fig. 3). For example, other attributes associated with the structure of GQVs (*e.g.*, dip data and kinematic indicators), their geochemistry (*e.g.*, whole-rock and stable isotopes), and their fluid inclusion data may be included. Furthermore, the cartographic trace of specific GQVs may be modified based on new detailed geological mapping.

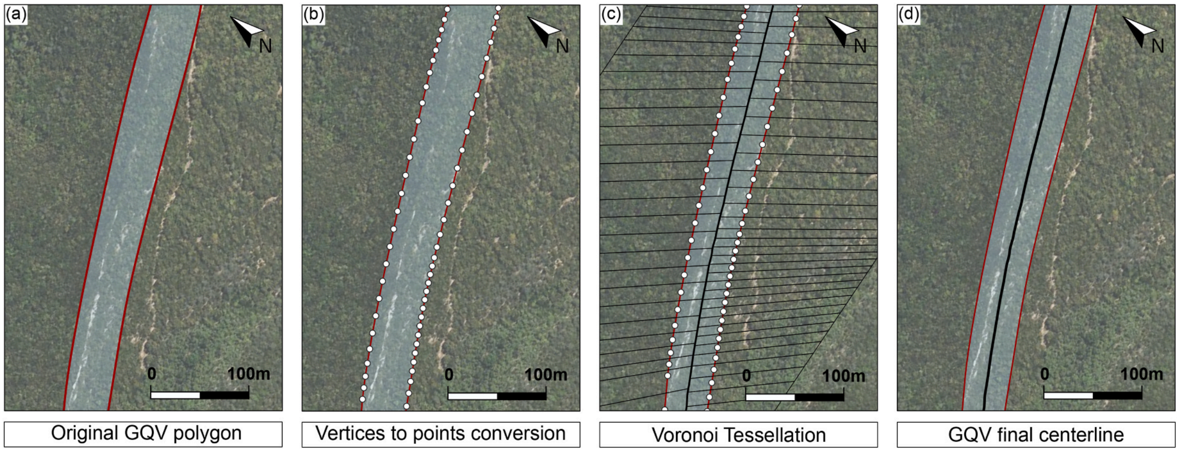

Fig. 4. Summary of the workflow to obtain the centrelines of the giant quartz vein polygons, from the original conversion of shape vertices into points (a, b) to the Voronoi Tessellation, peripheral trace lines removal, and final centreline obtention (c, d). This workflow is demonstrated by using the central sector of the Vein ID#501 (Roc de Frausa Massif, southwest Maçanet de Cabrenys town), partially visible from photogrammetric imagery. Map rotation is 55° westwards.

4.2. GQV location and host rock variability

The GQVs of the Pyrenees are chiefly located in the central and eastern parts of the chain, considering the sub-divisions of Miró et al. (2020) and Muñoz (2002) (Figs. 1, 2 and 6). However, other large quartz bodies also crop out westwards, in the Chiroulet-Lesponne sector and in the Bilbao Anticlinorium (Figs. 1 and 6). Most veins are widespread along the central part of the chain (Fig. 2) and thus hosted in the pre-Variscan basement (Fig. 6). Veins are not restricted to specific host rock types although the largest structures are mostly hosted in Variscan gneisses (n = 179) and late-Variscan intrusives (n = 244). The late-Neoproterozoic to Carboniferous metasedimentary succession that crops out extensively along the basement of the Pyrenees (Fig. 2) is also a common host rock type (n = 357), whilst the late Neoproterozoic, Ordovician and Permo-Carboniferous volcanic rocks only host four GQVs because of the reduced thickness and lateral extension of these volcanic rocks (Fig. 6).

Veins cropping out within the Alpine sedimentary cover of the Pyrenees are of special interest since their mere occurrence questions the assumption that the GQVs of the Pyrenees are Variscan in age. Although they are rarer than the GQVs in the Variscan and pre-Variscan rocks, a total of 93 GQVs in the NPZ and SPZ are hosted by Mesozoic and Cenozoic sedimentary and metamorphic rocks (Fig. 6). In the SPZ, they are only present at the southern slopes of the Albera and Roc de Frausa massifs, where they are hosted in Upper Cretaceous (Santonian to Campanian) sandstones and conglomerates, as well as within Eocene (Ilerdian) marlstones. In contrast, GQVs of the NPZ can be found in the Aglí, Arize, Trois-Seigneurs and Chiroulet-Lesponne massifs (Figs. 1, 2 and 6). In the northern slope of the Aglí Massif, along the St. Paul de Fenoillet syncline, GQVs are hosted either in Upper Triassic (Rhaetian) claystones, sandstones, dolostones and marlstones, in Jurassic (Hettangian) dolostones, limestones and marlstones, in Upper Jurassic-Lower Cretaceous (Kimmerdigian-Upper Aptian) limestones, rudist limestones and breccias, and in Paleogene (Eocene) breccias. However, in the southern slope of the Aglí Massif, GQVs are only present within the metamorphic zone along the Boucheville syncline, where they are hosted in hornfels formed during the HT-LP Cretaceous metamorphism (Fig. 6). Westwards, in the Arize – Trois-Signeurs Massif, two GQVs are hosted in Permian-Triassic detritic and Upper Cretaceous (Cenomanian-Coniacian) carbonate rocks, respectively, whilst a GQV is present within Upper Cretaceous (Cenomanian) carbonate rocks of the northern Chiroulet-Lesponne area. Finally, veins emplaced around the Bilbao Anticlinorium are hosted in Lower Cretaceous (Valanginian to Albian) carbonate and siliciclastic rocks.

4.3. Statistical-geometrical analysis

Most of the GQVs of the Pyrenees have an average width ranging between 10 and 60 m, regardless of their outcrop area or host rock type (Fig. 7). The violin plot of Fig. 7a shows that the average width (kernel density plots) displays two different distribution patterns depending on the GQV location. The first pattern, present at the Aston-Ospitalet, Canigó, Arize–Trois-Signeurs, Chiroulet-Lesponne and Mouthoumet massifs, consists of highly variable width values and a chiefly uniform distribution (Fig. 7a). It is characterised by large standard deviations and a strong difference between the median and mean values, suggesting the existence of outlier values in these sectors. This is confirmed when the average width values are plotted against the GQVs length (Fig. 7b). The second width pattern can be identified at the Millas, Cap de Creus, Albera, Castillion, Bilbao Anticlinorium, Aglí, Andorra-Montlluís and Roc de Frausa massifs. In contrast to the first width pattern, the GQV widths here are more constant and exhibit a broadly normal "bell-shaped" or bimodal distribution together with more constrained interquartile ranges (Fig. 7a). The Canigó and Roc de Frausa massifs, which have a similar number of data, represent two endmembers of the aforementioned patterns (Fig. 7c). Highly variable average width values are observed for the Canigó Massif, whilst more constant, mostly <40 m, average width values are found in the Roc de Frausa Massif (Fig. 7a, c).

When plotting the average width against the length of each GQV (Fig. 7b), it can also be observed that 60% of the investigated GQVs have a length between 20 and 1,000 m, whilst only few of them (4%) are longer than 1,500 m. Vein lengths do not correlate with the average widths, and most of the outlier width values correspond to veins shorter than 1,000 m (Fig. 7b). The longest GQVs mostly occur at the Canigó, Aglí, and Roc de Frausa massifs, whereas veins from the Chiroulet-Lesponne, Arize–Trois-Signeurs, Aston-Ospitalet, and Mouthoumet massifs tend to be shorter with lengths of about 20–600 m (Figs. 7b and 8). The cumulative distributions of GQV lengths in each representative sector also illustrate an upper length cut-off value at approximately 1,500 m (Fig. 8). In all cases, the cumulative frequency of veins with lengths lower than 200–300 m is high and there is a marked decrease in frequency for GQVs between 300 and 500 m long. The frequency plots for the Andorra-Montlluís (Fig. 8f), Millas (Fig. 8g), Canigó (Fig. 8h), and Roc de Frausa (Fig. 8j) massifs exhibit an almost horizontal slope when cumulative frequency values are high (corresponding to vein lengths below ca. 300 m). However, negative correlations can be envisaged even for low length values (ca. <100–200 m) at the Bilbao Anticlinorium (Fig. 8a), Castillion (Fig. 8c), Aston-Ospitalet (Fig. 8e) and Albera massifs (Fig. 8k).

On top of vein length and average width data, individual width

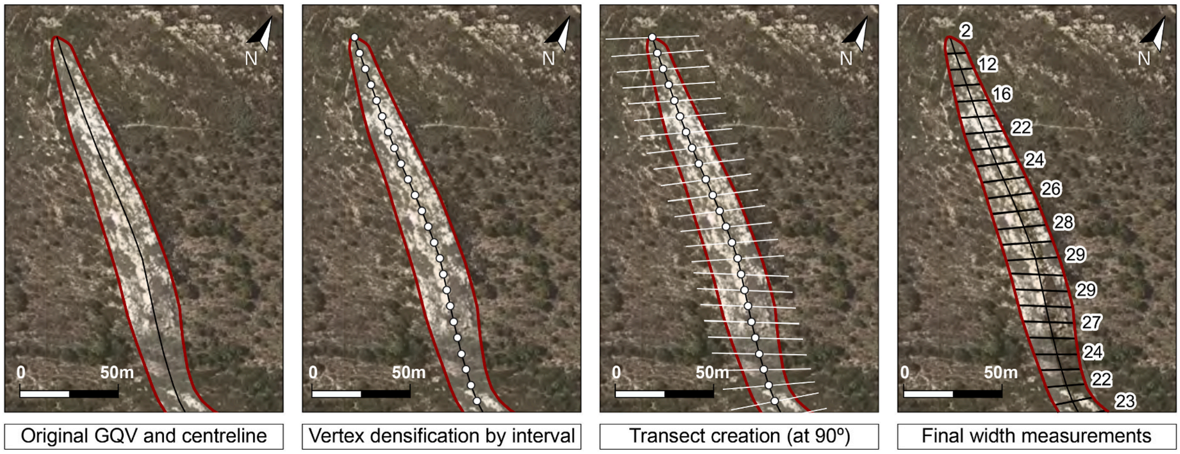

Fig. 5. Summary of the workflow to obtain the individual width values every 20 m along the veins strike. This workflow is illustrated with the north-western sector of the Vein ID#531 (Cap de Creus Massif, north Roses town). The resulting width dataset has been used to build Figs. 9 and 10.

measurements every 20 m along the strike of each single GQV were also acquired in order to address the width variations of individual veins (Figs. 5, 9 and 10). The width variability along representative veins from different outcropping sectors is plotted against distance in Fig. 9 for GQVs hosted in the basement and in Fig. 10 for veins hosted in the sedimentary cover of the Pyrenees. Pre-Variscan rocks (Fig. 9) have been classified among Variscan gneisses, Ediacaran–Carboniferous meta-sediments and Late-Variscan granitoids since these are the most common host rock types in the studied area (Figs. 2 and 6). The vein width is often variable along strike in veins hosted in basement rocks, regardless of the host rock type (Fig. 9). Especially, veins hosted either in gneisses or Late-Variscan intrusives have widths that vary between 40 and 60 m along the vein strike within just a few tens to hundreds of metres. These veins thus look like a string of connected lenses with narrow necks. However, some GQVs have the shape of a single lens with their width relatively constant for most of the vein, and then tapering off towards their terminations. In these cases, along-strike width values define a regular bell-shaped morphology. This width pattern is rare in the basement rocks where it is mostly found in GQVs hosted by Ediacaran to Carboniferous metasedimentary rocks, and only observed at the Aglí Massif (Fig. 9). The GQVs hosted in Mesozoic/Cenozoic sedimentary and metamorphic rocks show relatively regular widths along their strike (Fig. 10). It can be observed that widths remain relatively constant along the vein strike, except where the veins narrow towards their tips (Fig. 10). No difference is observed between the patterns for GQVs hosted by siliciclastic *vs.* carbonatic sediments (Fig. 10). It should, however, be noted that there are only a few veins in the NPZ and SPZ (Figs. 1, 2 and 6).

The GQV strike variations were also quantified (Fig. 11). The GQV traces (*i.e.*, their centrelines) were segmented into 44,052 segments to consider their along-strike orientation changes, and segments were classified according to their corresponding sector (Figs. 1 and 6). Host rock types (Fig. 6) were also considered as a classification criterion for strike analyses, although no correlations were found. If the location factor is considered and addressed from west to east (Figs. 1, 2 and 11), the GQVs outcropping in the Bilbao Anticlinorium show a chiefly constant NW-SE orientation (Fig. 11a). Eastwards, in the NPZ, a roughly WNW-ESE trend is found for veins located in the Chiroulet-Lesponne and Castillion massifs (Fig. 11b, c, respectively), whereas veins from the Arize-Trois-Signeurs Massif show a more constant WSW-ENE orientation (Fig. 11d). The Eastern Pyrenees is the most statistically representative sector for the analysis of GQV strike (Figs. 1, 2 and 11e-l). GQVs of the Aston-Ospitalet, Montlluís and Millas massifs (Fig. 11e-g, respectively) are mostly oriented WNW-ESE to NW-SE. The GQVs of the Canigó, Aglí and Roc de Frausa massifs, however, exhibit an almost W-E strike (Fig. 11h-j, respectively). However, several GQVs with orientations ranging from NNW-SSE to SSW-NNW are also noted in these sectors. Eastwards, in the Albera Massif (Fig. 11k), vein strikes range from SW-NE, whilst at the easternmost termination of the chain, in the Cap de Creus Massif (Fig. 11l), a dominantly constant NW-SE trend can be observed.

Strikes that deviate significantly from the dominant orientations can also be observed in some GQVs segments in all the sectors (Fig. 11). However, to avoid bias, the rose diagrams are plotted with the area of each bar of the plot proportional to the frequency of orientations (Healy et al., 2017). This shows that the orientations that differ from the main GQVs trend in each sector are scarce. The N–S-trending GQVs from the Andorra-Montlluís Massif (Fig. 11f), as well as that the SW-NE-trending GQVs from the Bilbao Anticlinorium (Fig. 11a), are good examples of how this bias produced by punctual outlier trends are outweighed.

If the strike of GQVs segments is plotted against the segment length, one can observe that the short (*i.e.*, $<$10 m) segments show a wide range of orientations, whilst larger ($>$10 m) GQV segments mostly trend SW-NE to NW-SE (Fig. 12). Curiously, the largest GQVs from the Canigó (Fig. 12h), Roc de Frausa (Fig. 12j) and Aston-Ospitalet (Fig. 12e) massifs show a constant E-W orientation, whilst strikes and segment lengths of the other sectors present more uniform distributions (Fig. 12a–d, f, g, i, k, l).

4.4. *Orogen-scale distribution patterns*

The orogen-scale density map shown in Fig. 13a reveals a clear clustering of GQVs at the central and eastern parts of the chain, as well as in the westernmost area, the Basque-Cantabrian Pyrenees. Three representative outcropping sectors have been selected to analyse the distribution patterns of GQVs in more detail: the Bilbao Anticlinorium in the westernmost Pyrenees (Fig. 13b), the Arize-Trois-Signeurs Massif in the Central Pyrenees (Fig. 13c), and the Canigó Massif in the eastern part of the chain (Fig. 13d).

GQVs of the Bilbao Anticlinorium are mostly clustered around NW-SE faults parallel to the main fold axis (Fig. 13b). These faults have been interpreted as a four main NE-directed thrusts that separate four allochthonous slices (from NE to SW): the Bilbao, Cegama, Aiztgorri and Villaro thrusts (Ábalos et al., 2008). Most veins are found along the Bilbao thrust, within the Aptian-Albian limestones, marls and sandstones (Urgonian and Supra-Urgonian) that constitute the Durango Slice (Ábalos et al., 2008; Ortiz and Perconig, 1975, Fig. 13b). This fault, formed during the Early Cretaceous rifting stage in the Basque-Cantabrian basin and later on reactivated during the Alpine compression (Ábalos et al., 2008 and the references therein), extends more than 120 km up to the NW of Pamplona (Fig. 1). However, GQVs are restricted to its north-western termination at the Cantabrian coast

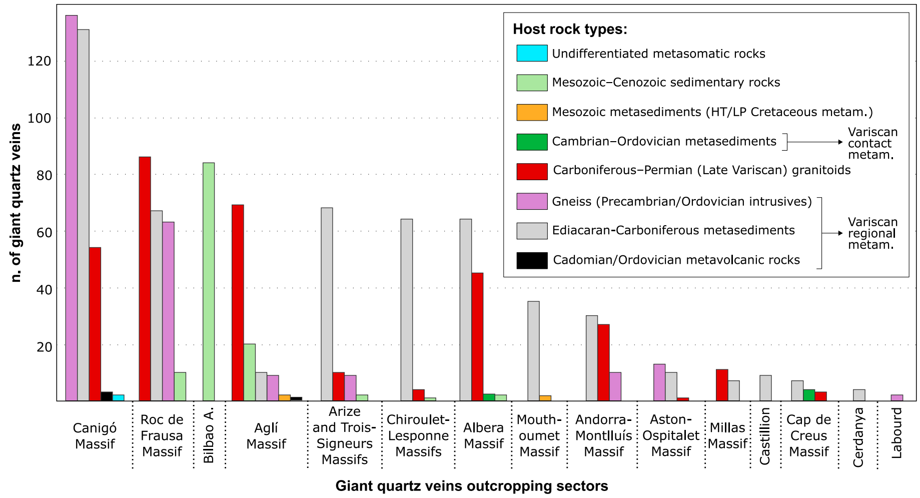

Fig. 6. Histogram showing the number of giant quartz veins and their host rock types that are indexed in each outcropping sector.

only (Fig. 13b).

In the Arize-Trois-Signeurs Massif, GQVs are in some cases related to regional faults and more often to the regional foliation (Fig. 13c). Vein trends of the Arize Massif range from SW-NE to W-E, and they are emplaced within pre-Silurian metapelites in the eastern sector, within the Arize gneiss in the southern area and within the Lacourt pluton and the Quercabanac hornfels in the westernmost zone. Southwards, WSW-ENE-striking GQVs of the Trois-Signeurs Massif are emplaced within the Trois-Signeurs granite and more often within the pre-Silurian metapelites, showing no relation with known faults (Fig. 13c).

The largest and widest GQVs of the Pyrenees are found in the Canigó Massif (Figs. 1b–f and 13d). They trend in an E-W direction and either crosscut Ediacaran—Lower Cambrian and Cambrian—Ordovician metasedimentary sequences, the Canigó gneisses, and the Carboniferous Costabona and Canigó granitoids (Figs. 6 and 13d). The largest structures are clustered in the southwestern sector of the Canigó gneiss and at their contact with the late Neoproterozoic and Lower Palaeozoic metasediments, although they extend discontinuously towards the east, where they crosscut the Costabona granite (Fig. 13d). At the northern sector of the Canigó Massif, other SW-NE or W-E GQVs are present. These quartz bodies are mostly located around the north-western contact between the Canigó granite and the Canigó gneisses, although they also extend discontinuously towards the east and west, along the entire northern sector of the Canigó Massif.

5. Discussion

5.1. GIVEPY database: strengths, limitations, and lessons

The method presented here for the indexation of regional geological structures has strengths and weaknesses that must be considered when using the database for future studies and geological interpretations. In the same way, these strengths and weaknesses have to be considered when replicating this method to build similar databases of other geological structures and other regions worldwide. In this sub-section, a selected number of assumptions that have been made for the workflow design are critically reviewed. We discuss aspects of the datasets and their interpretations that are accurate, and those which are biased but could be improved with further work. We also discuss aspects that are inherently biased and, therefore, have no remedy.

If it is mapped, it exists. — The geological maps used as the starting point for the building of the GIVEPY database have been developed by geological surveys and other institutions during the last century. The maps are digitalized and updated versions of older detailed field-based maps. Accordingly, we have assumed that if a vein is mapped in a specific area, it is because a geologist has been to that area and has identified it as such. We verified this assumption through ground-truthing and comparison with areal and satellite images. Field-based verifications were carried out to the GQVs mapped by Cirés et al. (1994a) in La Cerdanya (IGME), by Losantos et al. (1997) in the Cap de Creus Massif (ICGC), and by Guitard (1965) in the Canigó Massif (BRGM). The existence of other quartz bodies was verified with high-resolution orthophotographs and satellite imagery provided by ICGC and COAH (Table 1). It can be confirmed that the geological mapping of the source layer is accurate given the scale of work, even for the smaller GQVs that are <100 m length.

The "real" number of structures. — All the GQVs included in the geological maps shown in Table 1 have been considered for the overall assessment of their location, host rock variability, geometry, and distribution patterns along the Pyrenees. However, every surface-based study is limited to what is cropping out in the studied area. This bias must be considered during regional analyses of any geological structure, especially in fold-and-thrust settings where different outcrop sectors may represent rocks from different depths of the crust and that may have experienced their own unique deformation history. The veins are emplaced at different structural levels, with some of them thus cropping out, while most of them probably still buried or already eroded, and therefore biasing the observed orogen-scale distribution patterns.

Topographic effects. — The GQVs rarely crop out in areas with a flat topography, but rather in areas with hills, valleys, and other topographic features. GQVs themselves tend to modify surface topography due to their strong resistance to weathering compared to that of other rocks (Fig. 1b–f). The topographic irregularities are influenced by (among others) the lithology and structure of rocks (*i.e.*, rock unit thicknesses, vein width, dipping attitude, folding, thrusting), hydrographic networks, and human activity. These features may generate a sinuous trace of geological contacts, that must be considered as a bias in any analysis of the orientation and distribution of linear features, either GQVs, fractures or faults (*e.g.*, Peacock et al., 2019). Thus, there will always exist a number of trace segments biased by topographic effects. Working with large amounts (*i.e.*, thousands) of trace lines or trace segments should, however, minimize the inferred error and decipher the real parameters of the target structures (Figs. 11 and 12).

From sub-vertical to gently dipping structures. — Fieldwork carried out in selected GQVs has revealed that in some cases they are indeed vertical or sub-vertical structures (*i.e.*, the Esquerdes de Rojà GQVs in the Canigó Massif; Ayora and Casas, 1983). Some other veins are, however, moderately dipping structures that therefore show an apparent width at their intersection with the surface. For example, the Gréixer and Ger GQVs, from the La Cerdanya area, are emplaced parallel to south

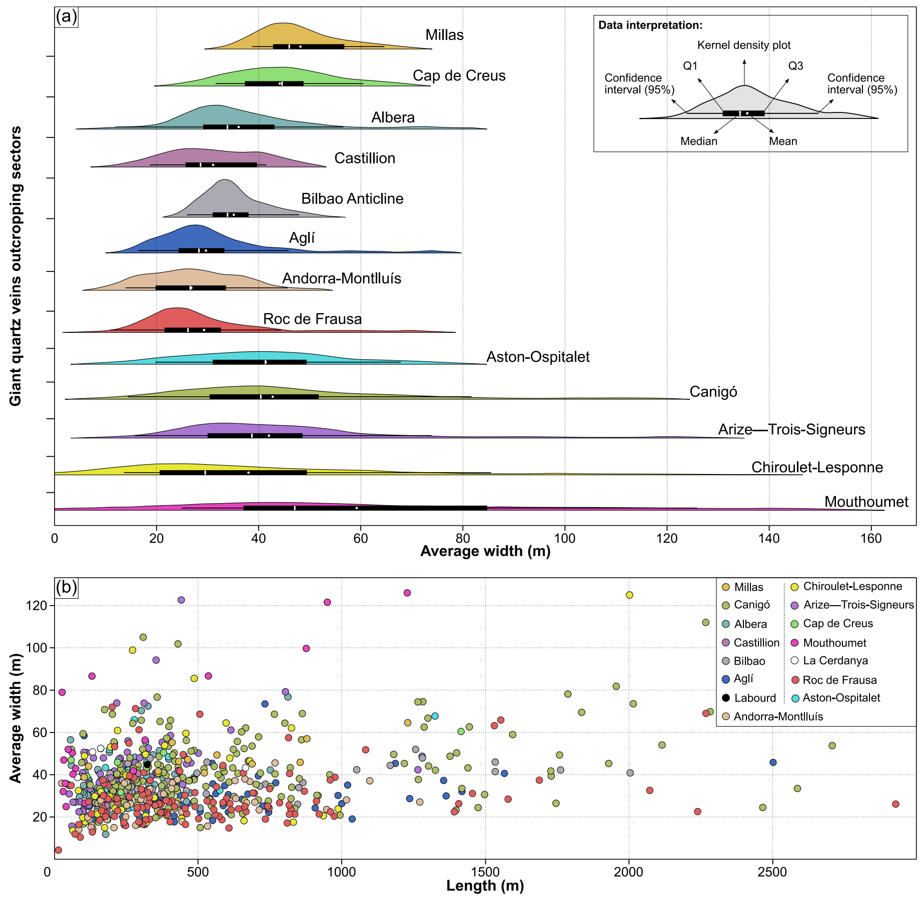

Fig. 7. (a) Violin plots (*i.e.*, kernel density distributions) of the average vein width values classified according to the outcropping sectors defined in Figs. 1, 2 and 6. (b) Average vein width values plotted against vein length and classified according to the same outcropping sectors as in (a).

verging thrusts that dip ~60° to the north (González-Esvertit et al., 2022), whilst the GQVs from Sant Miquel de Colera area are emplaced parallel to the regional cleavage and dip ~40-60° to the NE (Cirés et al., 1994a,b). Topographic effects mentioned above in this sub-section played a useful role in identifying the GQVs that are not sub-vertical, since their cartographic traces are often sinuous due to the surface irregularities. Given the low number (and length) of GQV traces that have been classified as biased by their dip and topographic intersections, this issue has not been addressed here. However, it must be considered if other geological structures with a gently to moderate dip (*e.g.*, faults or diagenetic alterations) are indexed and evaluated following the procedures suggested here.

Geological boundaries are inherently uncertain. — Field-derived geological data must not be perceived as objective results that are independent of any biases. From original delineation of geological boundaries during fieldwork to their digitalization in a GIS environment, there is an uncertainty that may depend on the working scale, the outcropping conditions, the interpretations of the surveyor, and even on the thickness of the pencil tip used (*e.g.*, Lark et al., 2015; Andrews et al., 2019 and references thereof). The original shape of the GQVs analysed in this study was corrected using aerial imagery to mitigate the inherent uncertainty of the original geological maps. This works well for the GQV, as they are easily recognizable by their unique bright white colour. Minimizing the uncertainty of the host rock types is, however, less straightforward because in most cases they are not easily inferred from topographic relief or colour variations on the surface. However, host rocks are treated in this work as one of the attributes of the GQVs and not as the main study target, and only one variable dependent on their cartographic uncertainty has been considered: in contact or not in contact with a GQV.

GQVs: chicken or egg? — Did the GQVs form along pre-existing brittle and ductile structures, or did these structures develop along the GQV strike due to their role as a mechanical flaw? Or even did the GQVs form syn-tectonically controlled by local deformation episodes at different sectors of the Pyrenees? It is widely known that veins are formed at zones of localized deformation, such as faults and fractures in the upper (brittle) crust and shear zones in the lower (ductile) crust (*e.g.*, Weisheit et al., 2013a, 2013b). Specifically in the Pyrenees, GQVs are emplaced following fold limbs, normal and reverse faults, and shear zones (Ayora et al., 1984; Casas, 1984, 1986; Le Bayon and Cochelin, 2020; González-Esvertit et al., 2022). Depending on their outcropping sector, the GQVs of the Pyrenees follow the direction of specific structures. We therefore suggest that it is more likely that the GQVs were mostly emplaced along different types of previously formed structures in each sector, rather than that the different types of structures were formed on the basis of the location of previous GQVs. The kinematic indicators and damage zones that have been observed affecting the GQVs may represent reactivation stages during successive deformational episodes after their formation or may even be the effect of the formation of the GQVs themselves (Bons, 2001). However, these issues are out of the scope of this work, and more field-based investigations on specific GQVs are necessary to decipher the complete deformational history for each case. Accordingly, we have so far avoided relating GQVs to particular deformation episodes in the GIVEPY database.

Beyond GQVs: application to other structures — Indexing geological structures other than veins can be achieved by following or adapting the workflow suggested here. The first aspect that must be considered is the working scale and the accuracy of the input layers (*i.e.*, original geological maps), as well as what the final product is intended to have. If both the original and final scales are the same, and the accuracy of the

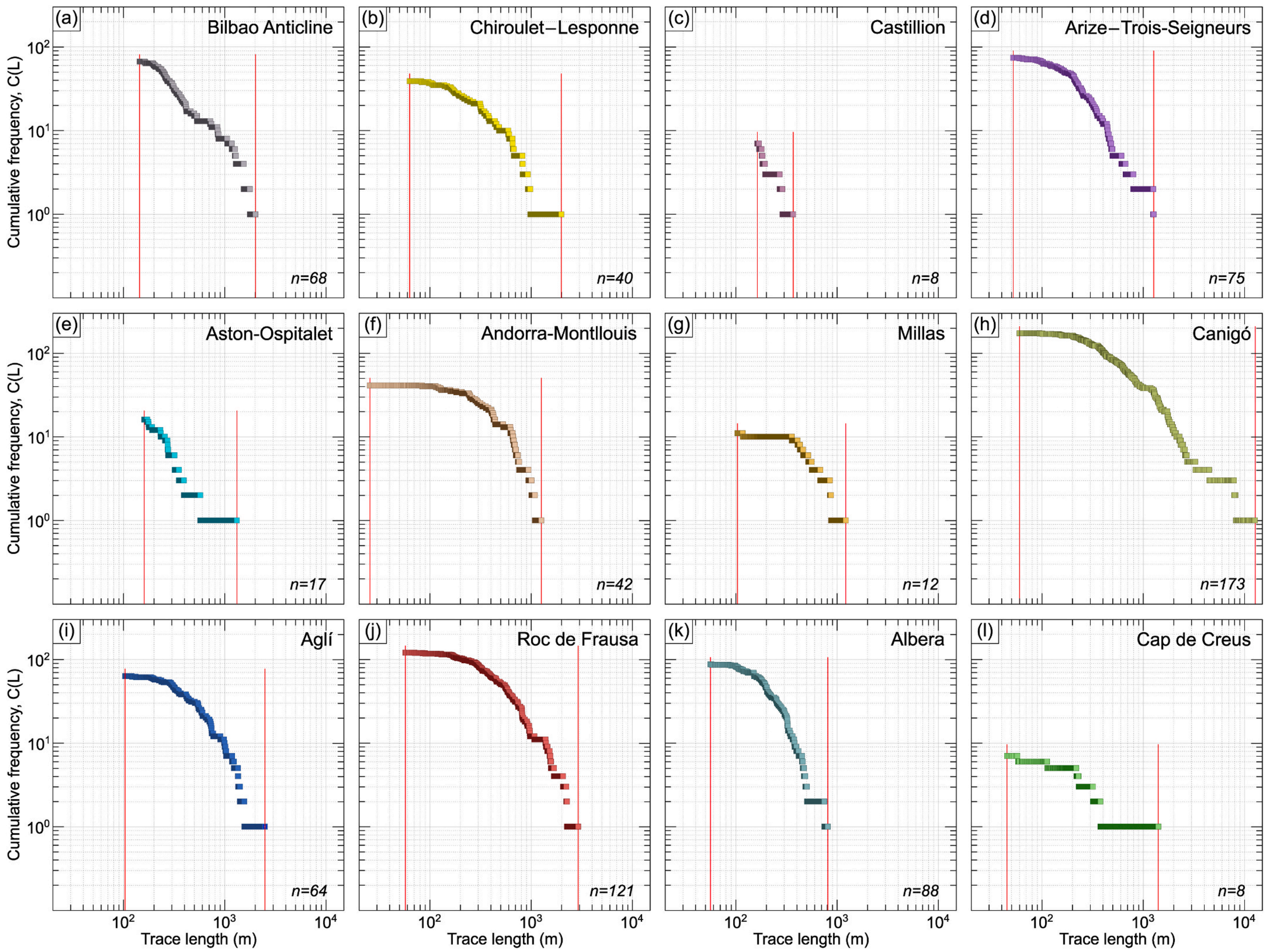

Fig. 8. Cumulative distribution frequencies of vein trace lengths classified according to the outcropping sectors defined in Figs. 1, 2 and 6.

input layers is high enough, then improvement by additional mapping (Fig. 3) may be omitted from the process. Otherwise, if one intends to obtain a final product with higher resolution than the source layers, satellite imagery, semi-automatic mapping or manual reshaping is required to improve the work scale (Fig. 3). The geometric expression of the targeted structures should also be considered. For example, for indexing linear features (*e.g.*, fold axes and cartographic traces of faults and shear zones), the process of centreline creation (Fig. 4) is not needed since the statistical-geometric analysis of these features can be achieved from its original geometry. Joining the attributes of the surrounding rocks by their location is, however, necessary for obtaining the faulted/sheared/folded rocks. Instead of the method used here for obtaining only the attributes of rocks directly in contact with the targeted structure (Fig. 3), a buffer of a certain distance from the targeted structure may be applied to consider a wider area. For polygon type features (*i.e.*, igneous intrusions, salt diapirs, dolomitized geobodies, etc.), the centreline creation may (or may not) be useful for deciphering the main structural trends. However, geometrical calculations as the outcropping area and, if the sub-surface is well known, the volume of the structure, are more likely to be useful. A buffer of a certain distance from the targeted structures may also be used in this case to obtain, for example, the overburden sequence around a salt diapir or the rocks that an igneous pluton intruded.

5.2. Regional structural controls on vein emplacement

As argued above in Sub-section 5.1, the GQV emplacement was likely controlled by structures that already existed. Different structures of the Pyrenees are the product of an asynchronous, multi-staged deformation history that includes pre-Variscan, Variscan, Cretaceous and Alpine tectono-metamorphic events, and that gave rise to the wide range of structure types and orientations that can be found along the chain today (Muñoz, 1992; Castiñeiras et al., 2008; Casas, 2010; Cochelin et al., 2017; Vacherat et al., 2017, among others). In this sub-section, relationships between the GQVs and other brittle and ductile regional structures are discussed for some of the main outcrop sectors. Structural data of GQV-related structures, obtained from the input layers (Fig. 3, Table 1), were plotted together with the GQV main trends for their comparison (Fig. 11). Furthermore, a review of available literature on each area was carried out to understand these relationships beyond the uncertainty of the structures mapped in the input layers.

Apart from the fact that the GQVs follow the NW-SE direction of the kilometric-scale Bilbao Anticlinorium in the westernmost Pyrenees (Fig. 13b), the GQVs strikes match the trend of several faults (Fig. 11a). These faults exhibit offsets of hundreds of metres and, according to García-Mondéjar and García-Pascual (1982), acted as fluid pathways for the formation of the GQVs in this area. Specifically, the Zaramillo-Artiba and Sasiburu-Pagasarri fault zones are related to quartz bodies with lengths of hundreds of metres to kilometres and widths of tens of metres.

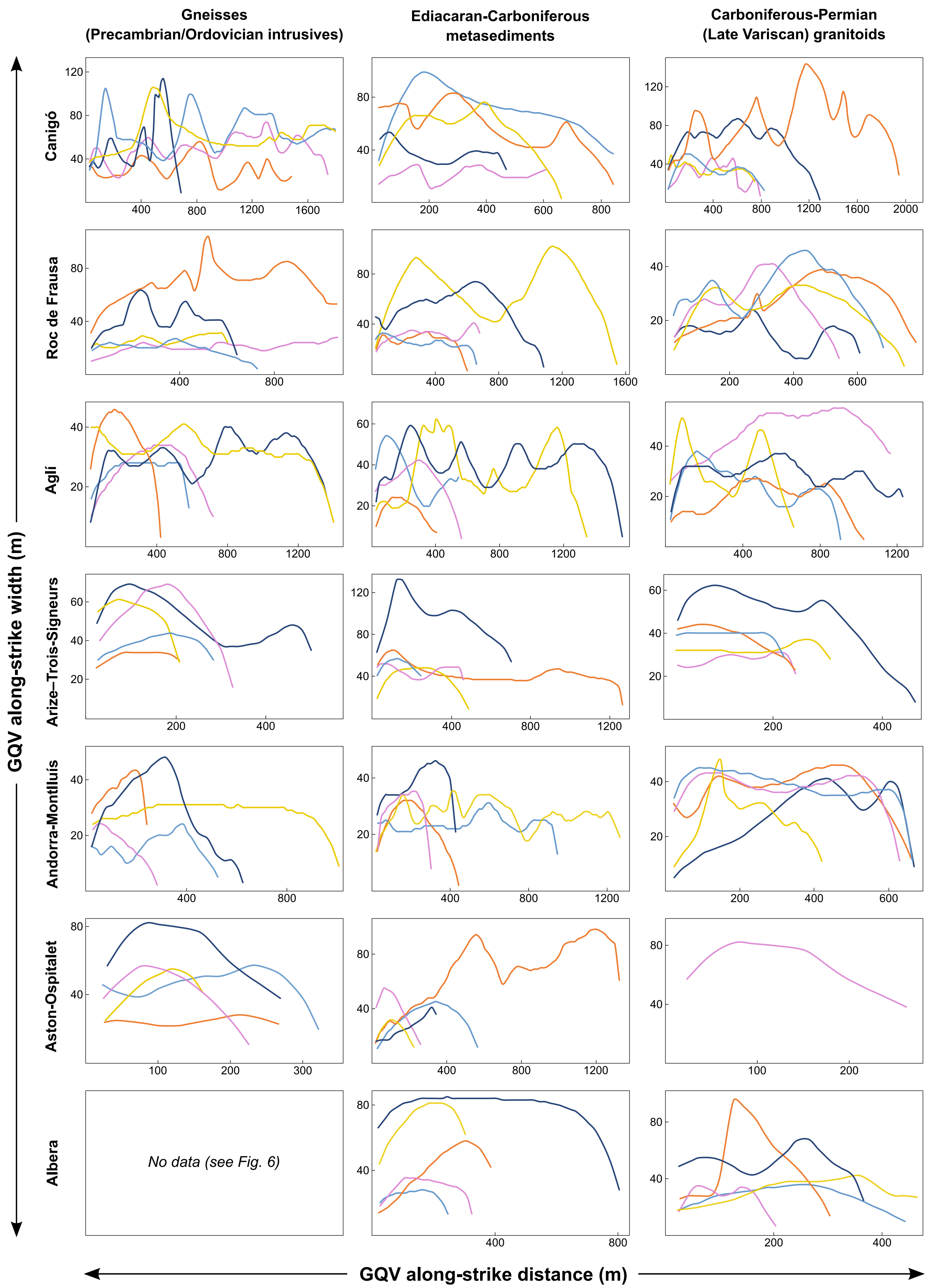

Fig. 9. Representative along-strike width variations classified according to the giant quartz vein outcropping sectors and the pre-Mesozoic host rock types. Each coloured line represents one vein. An along-strike distance of 200 m is highlighted with a discontinuous red line for comparison among the outcrop sectors. See Figs. 1 and 2 for location. (For interpretation of the references to colour in this figure legend, the reader is referred to the Web version of this article.).

Furthermore, the GQVs of the Bilbao Anticlinorium are affected by a regionally widespread foliation that strikes NW-SE and has a subvertical to steep NE dip (García-Mondéjar and García-Pascual, 1982; Ábalos et al., 2008). This foliation is found over a considerable area of the Durango allochthonous slice at the southwestern sector of the city of Bilbao (Ortiz and Perconig, 1975; García-Mondéjar and García-Pascual, 1982). Considering that these authors proposed a Lutetian age (ca. 48 to 41 Ma) for the foliation development and that the GQVs should postdate

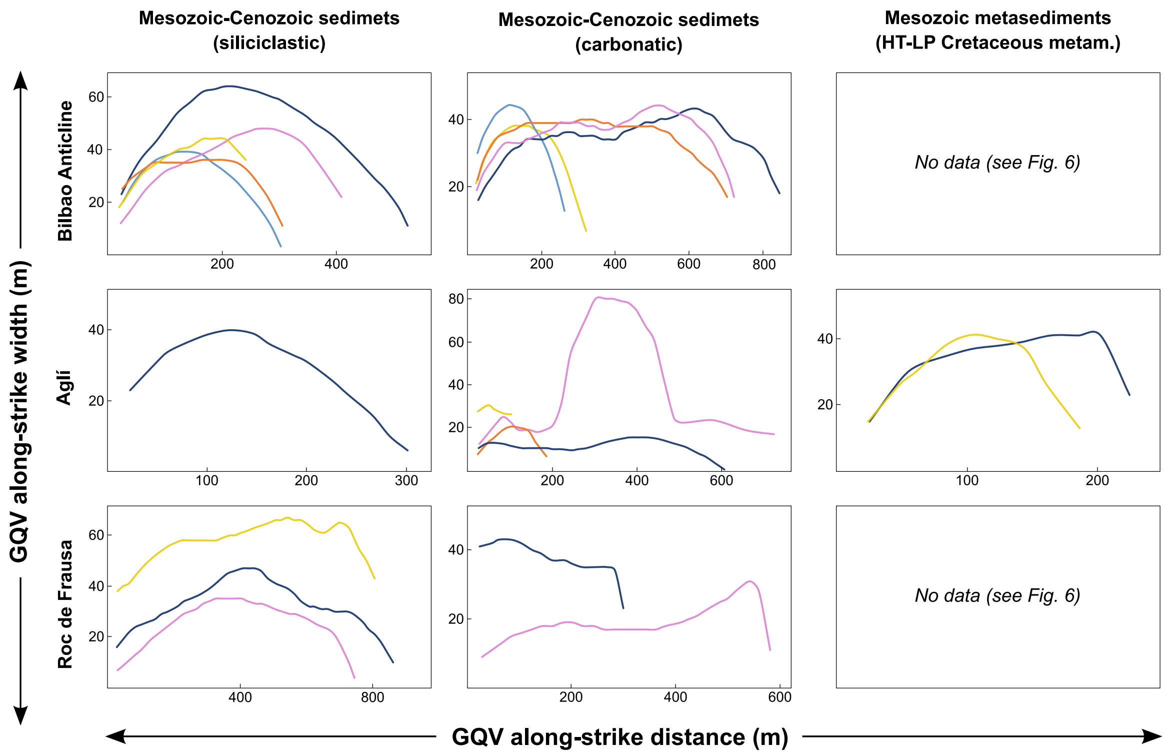

Fig. 10. Representative along-strike width variations classified according to the giant quartz vein outcrop sectors and the Mesozoic-Cenozoic host rock types. Each coloured line represents one vein. An along-strike distance of 200 m is highlighted with a discontinuous red line for comparison among the outcropping sectors. See Figs. 1 and 2 for location. (For interpretation of the references to colour in this figure legend, the reader is referred to the Web version of this article.).

the minimum age of the normal faults (Fig. 11a), the GQVs outcropping in the Bilbao Anticlinorium should be Late Cretaceous to Early Eocene in age.

GQVs of the Chiroulet-Lesponne massifs (Fig. 13c) are mostly found in the Lesponne area following the main thrusts and are mostly hosted by pre-Variscan metasedimentary rocks. Strikes of these faults vary as much as those of the GQVs, but show a main NW-SE trend with occasional N–S to WSW-ENE variations (Fig. 11b). According to Cochelin et al. (2021) and Lemirre et al. (2019) these thrusts are Alpine in age. Therefore, these GQVs could be pre-Alpine (Variscan), if it is assumed that their location controlled the development of Alpine thrusts along the entire massif, or more likely Alpine, presuming that their formation took place along previously formed thrusts.

Westwards, in the Arize—Trois-Signeurs Massif, GQVs are chiefly parallel to the E-W-trending foliation when emplaced within pre-Silurian metasediments, according to the structural data from the geological map of BRGM-D09 (Table 1) and the structural map of Cochelin et al. (2017). This foliation is interpreted as Variscan in age and linked to the regional metamorphism “D2” phase (*e.g.*, Poitrenaud et al., 2020). Some GQVs of this area are also emplaced along undifferentiated faults, either when emplaced within pre-Silurian metasediments or late-Variscan granitoids. These faults have never been interpreted in the literature nor in the geological maps of Table 1 and, therefore, the age of these GQVs remains undetermined.

GQVs of the Canigó Massif postdate the emplacement of the Costabona granite (Ayora and Casas, 1983; Casas, 1986) (Fig. 13d), which has been dated at 285.4 ± 2.2 Ma (Cocherie et al., 2005; unpublished report of the BRGM) and 302 ± 4 Ma (Laumonier et al., 2015). Their age should therefore be younger than Early Permian. Le Bayon and Cochelin (2020) suggested that some veins are linked to normal faults, Permian or Cretaceous in age, whereas Laumonier et al. (2015) define these faults as superimposed on quartz veins, arguing that the quartz is occasionally affected by a low-temperature mylonitic foliation as also identified by Casas (1986). This foliation can be correlated with other mylonitic belts found across the Pyrenees and, according to Carreras et al. (1980), was formed during a late Hercynian folding episode. There is, however, no general consensus about the age and origin of the normal faults of the Canigó Massif and their relationship with the GQVs. The age and structural controls on the emplacement of these veins, which are the largest ones cropping out in the Pyrenees, need further investigation.

In the easternmost Pyrenees, the Cap de Creus Massif exhibits discontinuous NW-SE trending quartz bodies that are emplaced along regional fractures of unknown age and kinematics, according to the geological maps of ICGC (Table 1). The age and origin of these GQVs cannot be constrained by the relative ages of the associated structures and their cross-cutting relationships, mainly because fold axial surfaces, shear zones, and fractures corresponding to different deformational events exhibit a similar NW-SE trend around the GQVs (*e.g.*, Carreras, 2001; Druguet et al., 2014; Losantos et al., 1997). What can be affirmed is that these GQVs postdate a Neoproterozoic-Lower Cambrian psammitic-pelitic metasedimentary sequence as well as the Roses (290.8 ± 2.9 Ma; Druguet et al., 2014) and Rodes granitoids, and exhibit (and thus predate) a mylonitic foliation that is folded by NW-SE-trending folds with a sub-vertical to SW-verging axial surface (Ayora et al., 1984; Carreras et al., 2006). This foliation is related to the development of the northern and southern shear belts of the Massif (Carreras, 2001; Druguet and Carreras, 2019), whose age and kinematics have been recently under discussion due to the Middle Jurassic and Tertiary $^{40}Ar/^{39}Ar$ muscovite ages proposed for shear zones from the northern shear belt (Vissers et al., 2017; Druguet et al., 2018; Oriolo et al., 2018). Alternatively, Carreras et al. (2004) suggested that the emplacement of the GQVs occurred contemporaneously to the mylonitization, under greenschist facies metamorphic conditions. On the basis of field analysis, Fonseca et al. (2015) identified two mylonitic foliations postdating the Roses-Palau GQV (southern Cap de Creus Massif) and proposed, on the basis of regional comparisons, that at least part of the deformation history recorded in the Roses Vein could be Alpine in age. Llorens et al. (2013) described shear zones affecting the Roses granodiorite and

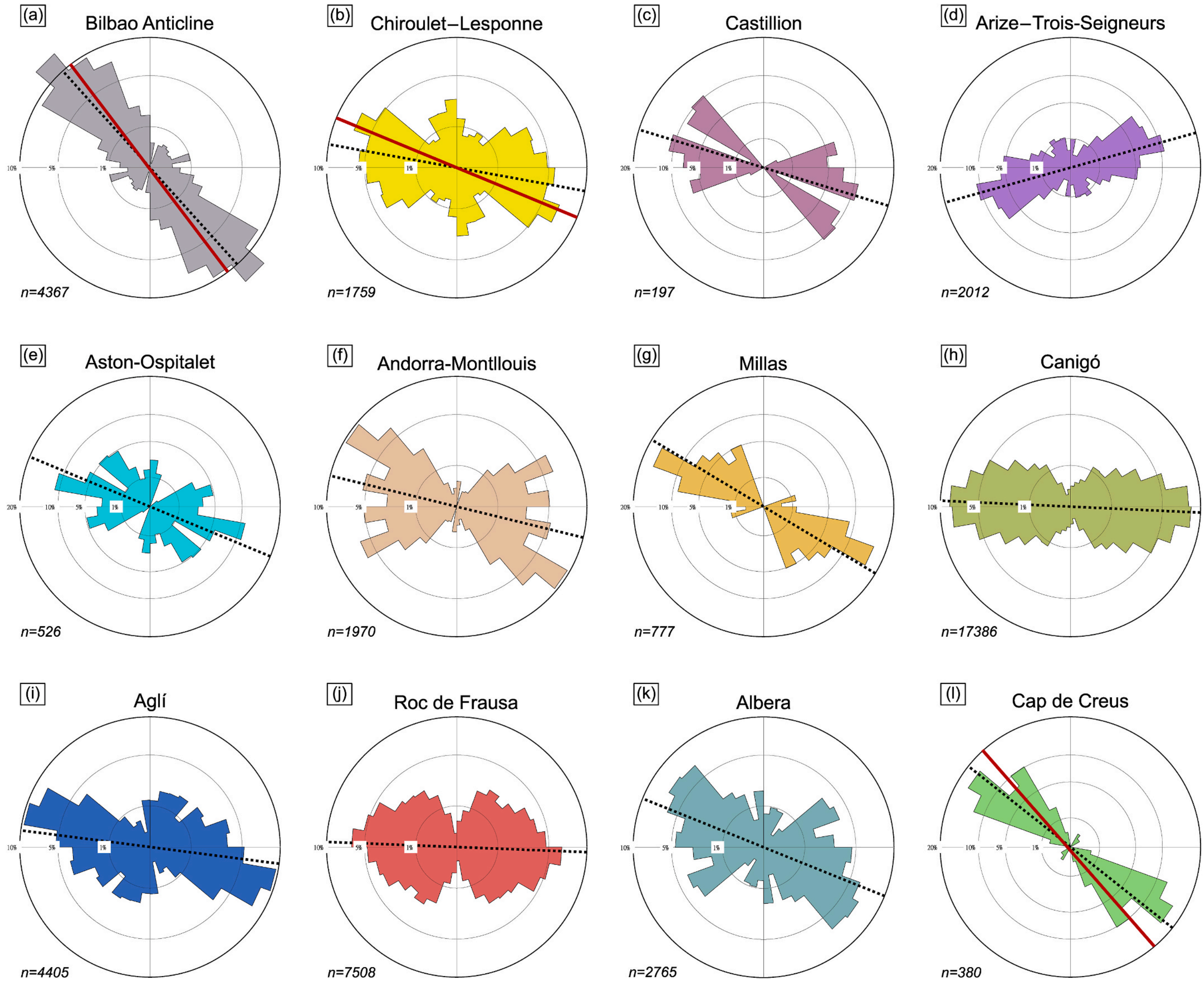

Fig. 11. Rose plots showing the strike of giant quartz vein segments according to their outcrop sector. See Figs. 1 and 2 for their location. The area of each bar of the plot is proportional to the orientation frequency. Red lines in (a), (b) and (l) represent the strike of vein-related structures cropping out in these sectors as discussed on Sub-section 5.2. (For interpretation of the references to colour in this figure legend, the reader is referred to the Web version of this article.).

estimated a high shear strain from unfolded folds, that also predate the formation of GQVs. Challenging the shear zone ages of Vissers et al. (2017), Druguet et al. (2018) highlighted, from a structural and palaeogeographical approach, that their results may been biased due to the partial resetting of the ^{40}Ar/^{39}Ar system following Meso-to Cenozoic thermal events. The Ar closure in muscovite can occur between 250 and 400 °C (Druguet et al., 2018), a temperature range that fits well with the 200–350 °C interval at which GQVs are believed to form (*e.g.*, Bons, 2001; Tannock et al., 2019). We thus propose that, in addition to the Variscan tectono-metamorphic events, these Meso-to Cenozoic thermal events may also have played an important role in creating favourable conditions for GQV emplacement along pre-existing Variscan structures. The active discussion on the influence of post-Variscan deformation in the Cap de Creus Massif deserves attention and will provide more insights into the age and mechanisms of GQV formation.

6. Conclusions

Here we proposed a workflow for indexing, organizing, and analysing the giant quartz veins of the Pyrenees, whose origin, formation mechanisms, and significance are not fully understood. Veins are hosted in a great variety of rocks, from late Neoproterozoic to Carboniferous metasedimentary rocks, to Variscan gneisses, late-Variscan granitoids, and Mesozoic to Cenozoic sedimentary rocks. The vein strikes range from SE-NW to SW-NE, and they are mainly found in the central and eastern parts of the chain. Frequently, the giant quartz veins are emplaced in association with other regional structural features such as cleavage, thrust faults, folds limbs or shear zones, which may provide insight into the regional structural controls on vein emplacement in the different Pyrenean domains, as well as their relative age. The largest and widest veins are located in the Canigó Massif, although other quartz bodies with lengths of hundreds of metres to kilometres are also ubiquitous along the chain, from its easternmost sector, the Cap de Creus Massif, to the westernmost end, the Basque-Cantabrian area. The resulting datasets are provided as a (interactive) Findable, Accessible, Interoperable and Reusable database that aims to serve as a starting point for boosting the regional and local understanding of these impressive structures.

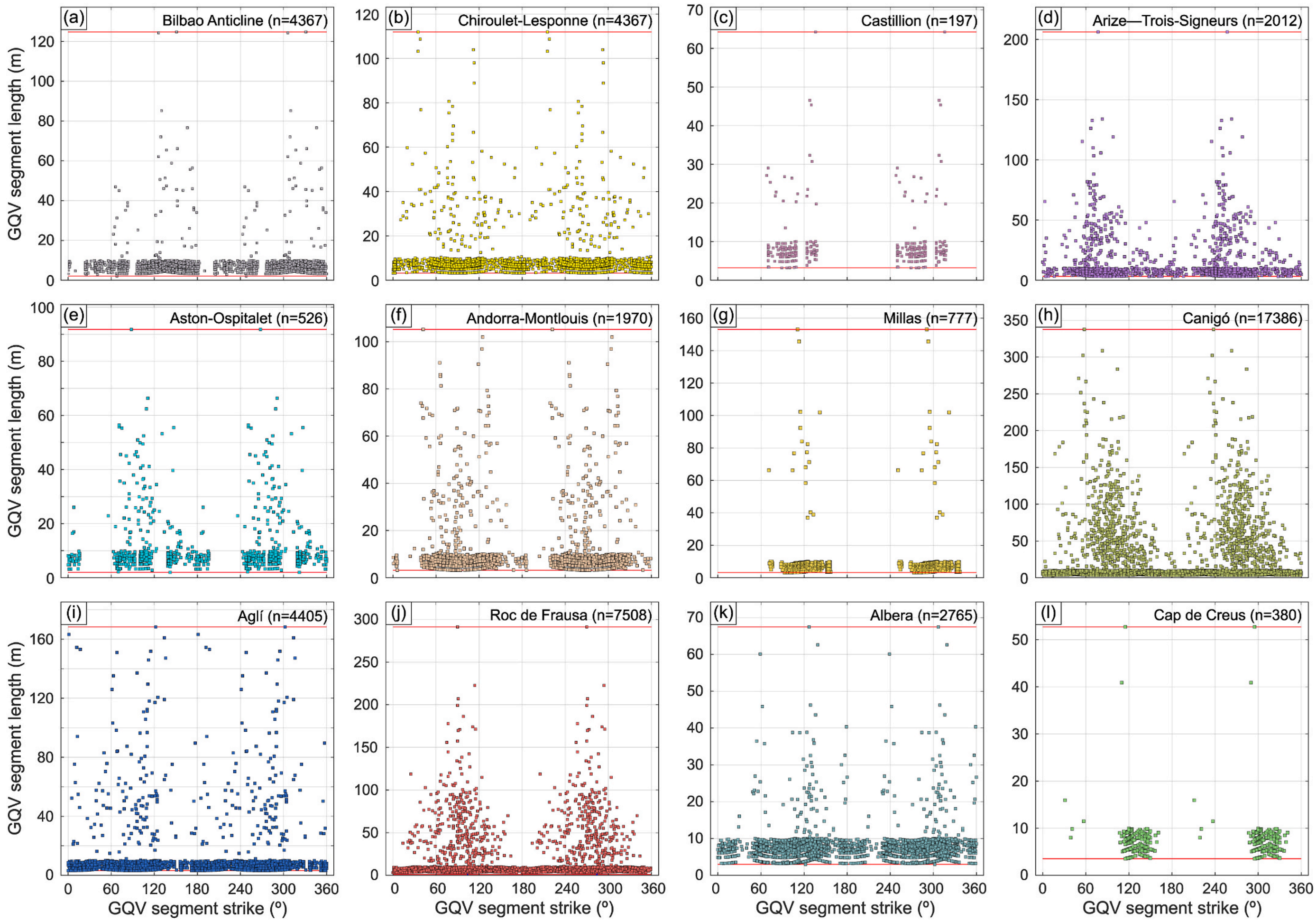

Fig. 12. Trace segment lengths plotted against their corresponding strike in each giant quartz vein outcrop sector. A segment length distance of 40 m is highlighted with a discontinuous red line for comparison among the outcropping sectors See Figs. 1 and 2 for location. (For interpretation of the references to colour in this figure legend, the reader is referred to the Web version of this article.).

Compiling the available information of geological structures is essential for the development of geoscientific knowledge, including that in structural geology and tectonics. The acquisition of their geological information, often available and accurate but scattered, typically incurred high costs in terms of economic resources and research time from the public and private sectors. Taking advantage of open-access data, and considering the assumptions made during the workflow design as well as the discussed strengths and possible bias, the proposed method is suitable for its application to different types of regional geological structures that are common targets of both academic and industry research.

Author statement

Eloi González-Esvertit: Conceptualization, Data curation, Methodology, Software, Formal analysis, Validation, Visualization, Writing - Original draft., Àngels Canals: Conceptualization, Supervision, Validation, Writing - Reviewing and Editing, Paul D. Bons: Supervision, Validation, Writing - Reviewing and Editing, Josep Maria Casas: Supervision, Validation, Writing - Reviewing and Editing, Enrique Gomez-Rivas: Conceptualization, Methodology, Supervision, Validation, Writing - Reviewing and Editing, Funding acquisition.

Data availability

The GIVEPY database follows the FAIR principles of data management. It is Findable and Accessible at the GIVEPY official webpage: https://givepy.info. Datasets, either in shapefile or .xlsx format, can be Interoperated and Reused after their download from the Zenodo data repository (CNRS-OpenAIRE), where a Digital Object Identifier (DOI) is assigned to make them citable and trackable:

- *Full Dataset (ESRI® Shapefile)* — (González-Esvertit et al., 2021b) — https://doi.org/10.5281/zenodo.5720513.

- *Full Dataset (MS Excel spreadsheet)* — (González-Esvertit et al., 2021c) — https://doi.org/10.5281/zenodo.5720604.

- *Vein* width *Dataset (MS Excel spreadsheet)* — (González-Esvertit et al., 2021d) — https://doi.org/10.5281/zenodo.5720630.

Furthermore, the GIVEPY database can be operated in any device with internet connection since an interactive map has been set up into the open-access QGIS Cloud Server: https://givepy.info/map-2/; aiming to facilitate GQVs targeting by interactive visualization during further research and teaching.

Declaration of competing interest

The authors declare that they have no known competing financial interests or personal relationships that could have appeared to influence the work reported in this paper.

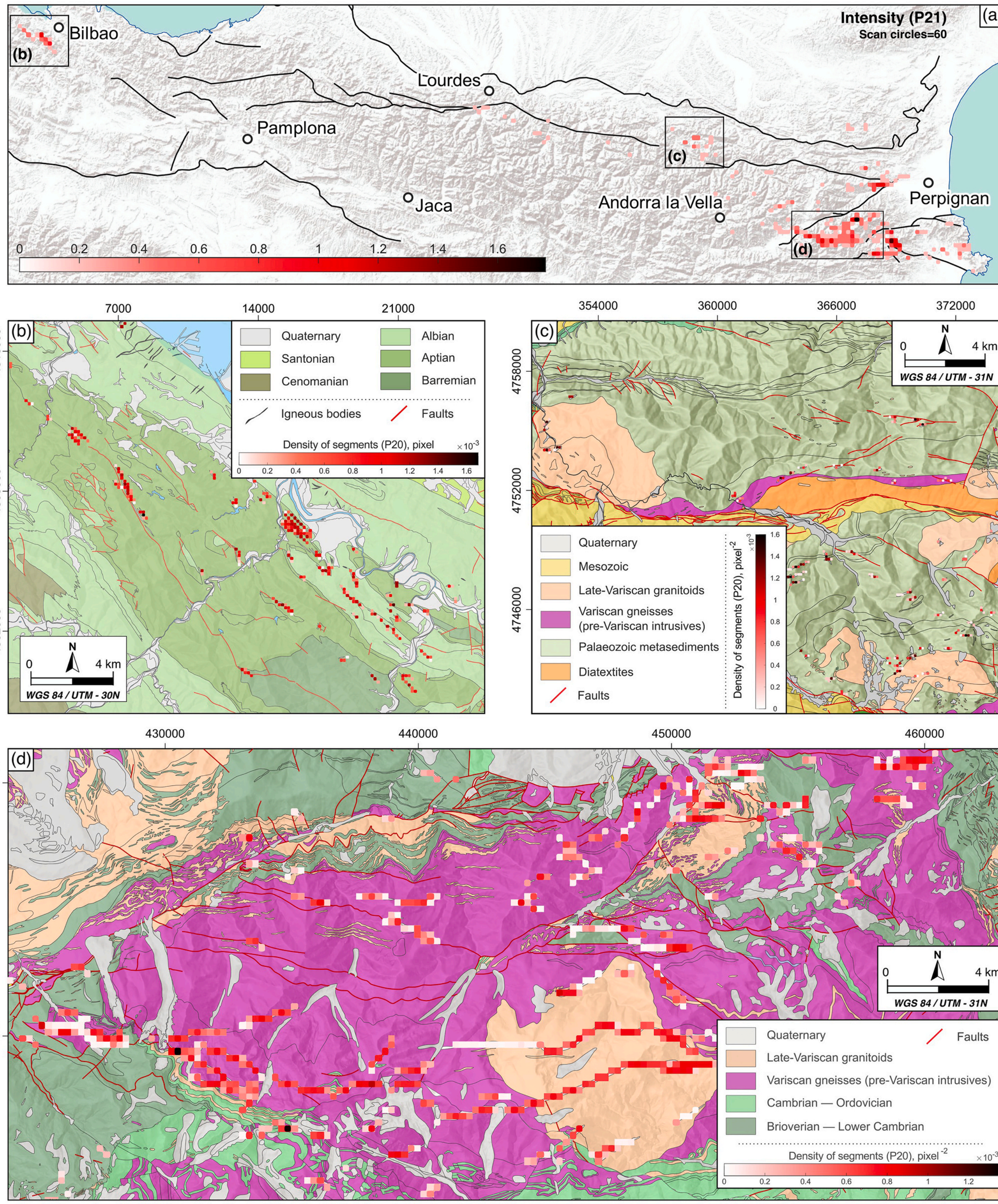

Fig. 13. Orogen-scale density map showing the distribution of the 741 giant quartz veins indexed in the GIVEPY database (a) and detailed geological maps of the Bilbao Anticlinorium (b), Chiroulet-Lesponne (c) and Canigó (d) outcrop sectors with their corresponding vein density maps. Number of scan circles has been set at 120 in all cases.

Acknowledgements

We would like to thank Manish A. Mamtani and an anonymous reviewer for their insightful revisions and suggestions, and Sandra McLaren and Virginia Toy for handling the Virtual and Digital Structural Geology Special Issue. The geological surveys of Catalunya (ICGC), Spain (IGME), Andorra (IEA-CENMA), and France (BRGM) are acknowledged for providing the accurate and complete datasets used as starring point. This work is a contribution to the 2017SGR-824 Research Group and to research projects DGICYT CGL2017-87631-P, PGC2018-

093903-B-C22 and PID2020-118999 GB-I00 funded by the Spanish Ministry of Science and Innovation (MCIN)/State Research Agency of Spain (AEI)/10.13039/501100011033. The PhD grant of EGE is funded by the Generalitat de Catalunya and the European Social Fund (2021 FI_B 00165). EGR acknowledges the "Ramón y Cajal" fellowship RYC2018-026335-I, funded by the Spanish Ministry of Science and Innovation (MCIN)/State Research Agency of Spain (AEI)/European Regional Development Fund (ERDF)/10.13039/501100011033.

Appendix A. Supplementary data

Supplementary data to this article can be found online at https://doi.org/10.1016/j.jsg.2022.104705.

References

Ábalos, B., Alkorta, A., Irίbar, V., 2008. Geological and isotopic constraints on the structure of the Bilbao anticlinorium (Basque–Cantabrian basin, North Spain). J. Struct. Geol. 30, 1354–1367. https://doi.org/10.1016/j.jsg.2008.07.008.

André, A.-S., Sausse, J., Lespinasse, M., 2001. New Approach for the Quantification of Paleostress Magnitudes: Application to the Soultz Vein System (Rhine Graben, France), vol. 17.

Andrews, B.J., Roberts, J.J., Shipton, Z.K., Bigi, S., Tartarello, M.C., Johnson, G., 2019. How do we see fractures? Quantifying subjective bias in fracture data collection. Solid Earth 10, 487–516. https://doi.org/10.5194/se-10-487-2019.

Autran, A., Guitard, G., 1968. Carte géologique détaillée de la France à 1/80.000: Prades. BRGM Service de la Carte Géologique de France.

Ayora, C., Carreras, J., Casas, J.M., Liesa, M., 1984. Informe Quarsos. Internal Report of the University of Barcelona. Universitat de Barcelona, Barcelona (available under request).

Ayora, C., Casas, J.M., 1983. Estudi microtermomètric dels filons de quars de les Esquerdes de Rojà, Massís de Canigó, Pirineu Oriental. Acta Geol. Hisp. 18, 35–46.

Boiron, M.-C., Cathelineau, M., Banks, D.A., Fourcade, S., Vallance, J., 2003. Mixing of metamorphic and surficial fluids during the uplift of the Hercynian upper crust: consequences for gold deposition. Chem. Geol. 194, 119–141. https://doi.org/10.1016/S0009-2541(02)00274-7.

Bons, P.D., 2001. The Formation of Large Quartz Veins by Rapid Ascent of ¯uids in Mobile Hydrofractures, vol. 17.

Bons, P.D., 2000. The formation of veins and their microstructures. J. Virtual Explor. https://doi.org/10.3809/jvirtex.2000.00007, 02.

Bons, P.D., Elburg, M.A., Gomez-Rivas, E., 2012. A review of the formation of tectonic veins and their microstructures. J. Struct. Geol. 43, 33–62. https://doi.org/10.1016/j.jsg.2012.07.005.

Candela, P.A., Piccoli, P.M., 2005. Magmatic processes in the development of porphyry-type ore systems. One Hundredth Anniversary. https://doi.org/10.5382/AV100.03. Society of Economic Geologists.

Canérot, J., Hudec, M.R., Rockenbauch, K., 2005. Mesozoic diapirism in the Pyrenean orogen: salt tectonics on a transform plate boundary. AAPG (Am. Assoc. Pet. Geol.) Bull. 89, 211–229. https://doi.org/10.1306/09170404007.

Carreras, J., 2001. Zooming on northern Cap de Creus shear zones. J. Struct. Geol. 23, 1457–1486. https://doi.org/10.1016/S0191-8141(01)00011-6.

Carreras, J., Druguet, E., Griera, A., Soldevila, J., 2004. Strain and deformation history in a syntectonic pluton. The case of the Roses granodiorite (Cap de Creus, Eastern Pyrenees). Geological Society, London, Special Publications 224, 307–319. https://doi.org/10.1144/GSL.SP.2004.224.01.19.

Carreras, J., Julivert, M., Santanach, P., 1980. Hercynian myionite belts in the eastern Pyrenees: an example of shear zones associated with late folding. J. Struct. Geol. 2, 5–9.

Carreras, J., Losantos, M., 1982. Geological setting of the Roses gtanodiorite (E-Pyrenees, Spain). Acta Geol. Hisp. 4, 211–217.

Carreras, J., Losantos, M., Palau, J., Escuer, J., 2006. Memoria asociada al mapa de la hoja 259 (Rosas) del Mapa Geológico de España. Instituto Geológico y Minero de España (IGME) - Serie MAGNA50.

Casas, J.M., 2010. Ordovician deformations in the Pyrenees: new insights into the significance of pre-Variscan ('sardic') tectonics. Geol. Mag. 147, 674–689. https://doi.org/10.1017/S0016756809990756.

Casas, J.-M., 1986. Shear bands and related extensional structures in a mylonitized quartz dyke. J. Struct. Geol. 8, 693–699. https://doi.org/10.1016/0191-8141(86)90074-X.

Casas, J.M., 1984. Estudi de la deformació en els gneis del massís del Canigó. PhD Thesis. Universitat de Barcelona, Unpublished, Barcelona, p. 284pp.

Casas, J.M., Castiñeiras, P., Navidad, M., Liesa, M., Carreras, J., 2010. New insights into the late ordovician magmatism in the eastern Pyrenees: U–Pb SHRIMP zircon data from the Canigó massif. Gondwana Res. 17, 317–324. https://doi.org/10.1016/j.gr.2009.10.006.

Casas, J.M., Navidad, M., Castiñeiras, P., Liesa, M., Aguilar, C., Carreras, J., Hofmann, M., Gärtner, A., Linnemann, U., 2015. The Late Neoproterozoic magmatism in the Ediacaran series of the Eastern Pyrenees: new ages and isotope geochemistry. Int. J. Earth Sci. 104, 909–925. https://doi.org/10.1007/s00531-014-1127-1.

Castiñeiras, P., Navidad, M., Liesa, M., Carreras, J., Casas, J.M., 2008. U–Pb zircon ages (SHRIMP) for Cadomian and Early Ordovician magmatism in the Eastern Pyrenees: new insights into the pre-Variscan evolution of the northern Gondwana margin. Tectonophysics 461 (1–4), 228–239. https://doi.org/10.1016/j.tecto.2008.04.005.

Chamberlain, K.J., Lehnert, K.A., McIntosh, I.M., Morgan, D.J., Wörner, G., 2021. Time to change the data culture in geochemistry. Nat. Rev. Earth Environ. 2, 737–739. https://doi.org/10.1038/s43017-021-00237-w.

Chauvet, A., 2019. Structural control of ore deposits: the role of pre-existing structures on the formation of mineralised vein systems. Minerals 9, 56. https://doi.org/10.3390/min9010056.

Cirés, J., Domingo, D., Sirvent, J.C., Santanach, P., Roca, E., Escuer, J., 1994a. Mapa geológico y Memoria de la Hoja n° 217 (Puigcerdà). In: Mapa Geológico de España E. 1:200.000 IGME.

Cirés, J., Morales, V., Liesa, M., Carreras, J., Escuer, J., Pujadas, J., 1994b. Mapa geológico y Memoria de la Hoja n° 220 (La Jonquera). In: Mapa Geológico de España E. 1:200.000 IGME.

Cochelin, B., Chardon, D., Denèle, Y., Gumiaux, C., Le Bayon, B., 2017. Vertical strain partitioning in hot Variscan crust: syn-convergence escape of the Pyrenees in the Iberian-Armorican syntax. Bull. Soc. Geol. Fr. 188, 39. https://doi.org/10.1051/bsgf/2017206.

Cochelin, B., Lemirre, B., Denèle, Y., Saint Blanquat, M., 2021. Strain partitioning within bending orogens, new insights from the variscan belt (Chiroulet-Lesponne domes, Pyrenees). Tectonics 40. https://doi.org/10.1029/2020TC006386.

Cocherie, A., Baudin, T., Autran, A., Guerrot, C., Fanning, C.M., Laumonier, B., 2005. U-Pb zircon (ID-TIMS and SHRIMP) evidence for the early ordovician intrusion of metagranites in the late Proterozoic Canaveilles Group of the Pyrenees and the Montagne Noire (France). Bull. Soc. Geol. Fr. 176, 269–282. https://doi.org/10.2113/176.3.269.

Cox, S.F., 1987. Antitaxial crack-seal vein microstructures and their relationship to displacement paths. J. Struct. Geol. 9, 779–787. https://doi.org/10.1016/0191-8141(87)90079-4.

de Riese, T., Bons, P.D., Gomez-Rivas, E., Sachau, T., 2020. Interaction between crustal-scale Darcy and hydrofracture fluid transport: a numerical study. In: Manning, A.H. (Ed.), Geofluids 1–14. https://doi.org/10.1155/2020/8891801, 2020.

Dey, T.K., Zhao, W., 2002. Approximate medial axis as a voronoi subcomplex. In: Proceedings of the Seventh ACM Symposium on Solid Modeling and Applications - SMA '02. ACM Press, Saarbr?cken, Germany, p. 356. https://doi.org/10.1145/566282.566333.

Dong, G., Morrison, G., Jaireth, S., 1995. Quartz textures in epithermal veins, Queensland; classification, origin and implication. Econ. Geol. 90, 1841–1856. https://doi.org/10.2113/gsecongeo.90.6.1841.

Druguet, E., Carreras, J., 2019. Folds and Shear Zones at Cap de Creus. Field Trip Guide XXXI Reunión de La Comisión de Tectónica - SGE 27.

Druguet, E., Carreras, J., Mezger, J.E., 2018. Discussion on 'middle jurassic shear zones at Cap de Creus (eastern Pyrenees, Spain): a record of pre-drift extension of the Piemonte–Ligurian ocean?' *Journal of the geological society, London* , 174, 289–300. J. Geol. Soc. 175, 187–188. https://doi.org/10.1144/jgs2017-042.

Druguet, E., Castro, A., Chichorro, M., Pereira, M.F., Fernández, C., 2014. Zircon geochronology of intrusive rocks from Cap de Creus, eastern Pyrenees. Geol. Mag. 151, 1095–1114. https://doi.org/10.1017/S0016756814000041.

Espínola, M.R., 1997. Estudi de l'hidrotermalisme associat a la granodiorita de Santa Coloma (Andorra). Unpublished Report (University of Barcelona.

Espínola, M.R., Soler, A., Arcos, D., Solé, J., 1997. Caracterización del hidrotermalismo durante la etapa de deformación alpina en el sector del valle de Bixessarri (Andorra). Boletín de La Sociedad Española de Mineralogía 20, 97–98.

Fagereng, Å., Diener, J.F.A., Meneghini, F., Harris, C., Kvadsheim, A., 2018. Quartz vein formation by local dehydration embrittlement along the deep, tremorgenic subduction thrust interface. Geology 46, 67–70. https://doi.org/10.1130/G39649.1.

Fisher, D.M., Brantley, S.L., 1992. Models of quartz overgrowth and vein formation: deformation and episodic fluid flow in an ancient subduction zone. J. Geophys. Res. 97, 20043 https://doi.org/10.1029/92JB01582.

Fonseca, H.A.M., Canals, A., Cirés, J., Casas, J.M., 2015. The roses giant quartz vein (Cap de Creus, eastern Pyrenees): geology and fluid inclusion data. Macla 20, 49–50.

Ford, M., Hemmer, L., Vacherat, A., Gallagher, K., Christophoul, F., 2016. Retro-wedge foreland basin evolution along the ECORS line, eastern Pyrenees, France. J. Geol. Soc. 173, 419–437. https://doi.org/10.1144/jgs2015-129.

Ford, M., Vergés, J., 2021. Evolution of a salt-rich transtensional rifted margin, eastern North Pyrenees, France. J. Geol. Soc. 178, jgs2019–j2157. https://doi.org/10.1144/jgs2019-157.

Fossen, H., Cavalcante, G.C.G., 2017. Shear zones – a review. Earth Sci. Rev. 171, 434–455. https://doi.org/10.1016/j.earscirev.2017.05.002.

García-Mondéjar, J., García-Pascual, I., 1982. Estudio geológico del anticlinorio de Bilbao entre los ríos Nervión y Cadagua. Koibe 12, 101–137.

González-Esvertit, E., Canals, À., Casas, J.M., Nieto, F., 2021a. Chlorite chemical adjustment in the Gréixer vein: effects on thermometry. Macla 25, 32–33.

González-Esvertit, E., Canals, À., Casas, J.M., Nieto, F., 2020. Insights into the structural evolution of the pre-Variscan rocks of the Eastern Pyrenees from La Molina quartz veins; constraints on chlorite and fluid inclusion thermometry. Geol. Acta 18, 1. https://doi.org/10.1344/GeologicaActa2020.18.18.

González-Esvertit, E., Gomez-Rivas, E., Canals, A., Casas, J.M., 2021b. Giant Quartz Veins of the Pyrenees Database - Full Dataset (ESRI Shapefile). https://doi.org/10.5281/ZENODO.5720513.

González-Esvertit, E., Gomez-Rivas, E., Canals, À., Casas, J.M., 2021c. Giant Quartz Veins of the Pyrenees Database - Full Dataset (MSExcel Spreadsheet). https://doi.org/10.5281/ZENODO.5720604.

González-Esvertit, E., Gomez-Rivas, E., Canals, À., Casas, J.M., 2021d. Giant Quartz Veins of the Pyrenees Database - Vein Width Dataset (MSEcxel Spreadsheet). https://doi.org/10.5281/ZENODO.5720630.
González-Esvertit, E., Molins-Vigatà, J., Canals, À., Casas, J.M., 2022. The Geology of the Gréixer Area (La Cerdanya, Eastern Pyrenees): Sardic, Variscan, and Alpine Imprints. Trab. Geol. In Press.
Guitard, G., 1970. Le métamorphisme hercynien mésozonal et les gneiss oeillés du massif du Canigou (Pyrénées orientales). Mémoires Du Bureau de Recherches Géologiques et Minières (BRGM) 63, 353.
Guitard, G., 1965. Carte Géologique des Massifs du Canigou et de la Carançà à 1/50.000. BRGM Service de la Carte Géologique de France.
Hasthorpe, J., Mount, N., 2007. The Generation of River Channel Skeletons from Binary Images Using Raster Thinning Algorithms, vol. 8.
Haunert, J.-H., Sester, M., 2004. Using the Straight Skeleton for Generalisation in a Multiple Representation Environment, vol. 11.
Healy, D., Rizzo, R.E., Cornwell, D.G., Farrell, N.J.C., Watkins, H., Timms, N.E., Gomez-Rivas, E., Smith, M., 2017. FracPaQ: a MATLAB™ toolbox for the quantification of fracture patterns. J. Struct. Geol. 95, 1–16. https://doi.org/10.1016/j.jsg.2016.12.003.
Holland, M., Saxena, N., Urai, J.L., 2009. Evolution of fractures in a highly dynamic thermal, hydraulic, and mechanical system - (II) Remote sensing fracture analysis, Jabal Shams, Oman Mountains. GeoArabia 14, 163–194. https://doi.org/10.2113/geoarabia1403163.
IGME-BRGM, 2009. Mapa Geológico de Pirineos 1, 400.000.
Kenis, I., Urai, J., Vanderzee, W., Hilgers, C., Sintubin, M., 2005. Rheology of fine-grained siliciclastic rocks in the middle crust—evidence from structural and numerical analysis. Earth Planet Sci. Lett. 233, 351–360. https://doi.org/10.1016/j.epsl.2005.02.007.
Lagabrielle, Y., Asti, R., Duretz, T., Clerc, C., Fourcade, S., Teixell, A., Labaume, P., Corre, B., Saspiturry, N., 2020. A review of cretaceous smooth-slopes extensional basins along the Iberia-Eurasia plate boundary: how pre-rift salt controls the modes of continental rifting and mantle exhumation. Earth Sci. Rev. 201, 103071 https://doi.org/10.1016/j.earscirev.2019.103071.
Lagabrielle, Y., Clerc, C., Vauchez, A., Lahfid, A., Labaume, P., Azambre, B., Fourcade, S., Dautria, J.-M., 2016. Very high geothermal gradient during mantle exhumation recorded in mylonitic marbles and carbonate breccias from a Mesozoic Pyrenean palaeomargin (Lherz area, North Pyrenean Zone, France). Compt. Rendus Geosci. 348, 290–300. https://doi.org/10.1016/j.crte.2015.11.004.
Lahiri, S., Rana, V., Bhatt, S., Mamtani, M.A., 2020. Paleostress and statistical analysis using quartz veins from mineralized and non-mineralized zones: application for exploration targeting. J. Struct. Geol. 133, 104006 https://doi.org/10.1016/j.jsg.2020.104006.
Lark, R.M., Lawley, R.S., Barron, A.J.M., Aldiss, D.T., Ambrose, K., Cooper, A.H., Lee, J. R., Waters, C.N., 2015. Uncertainty in mapped geological boundaries held by a national geological survey:eliciting the geologists' tacit error model. Solid Earth 6, 727–745. https://doi.org/10.5194/se-6-727-2015.
Laumonier, B., 2015. Les Pyrénées alpines sud-orientales (France, Espagne) – essai de synthèse, vol. 44.
Laumonier, B., Calvet, M., Bayon, B.L., Barbey, P., 2015. Notice explicative de la feuille Prats-de-Mollo-La-Preste à 1/50,000. BRGM Éditions-Service géologique national, p. 193.
Le Bayon, B., Cochelin, B., 2020. Anatomy of an extensional shear zone leading to the exhumation of the middle crust within the Canigou dome (Eastern Pyrenees, Axial Zone). J. Struct. Geol. 141, 104200 https://doi.org/10.1016/j.jsg.2020.104200.
Lee, D.T., 1982. Medial Axis transformation of a planar shape. IEEE Transactions on Pattern Analysis and Machine Intelligence PAMI- 4, 363–369. https://doi.org/10.1109/TPAMI.1982.4767267.
Lemarchand, J., Boulvais, P., Gaboriau, M., Boiron, M.-C., Tartèse, R., Cokkinos, M., Bonnet, S., Jégouzo, P., 2012. Giant quartz vein formation and high-elevation meteoric fluid infiltration into the South Armorican Shear Zone: geological, fluid inclusion and stable isotope evidence. J. Geol. Soc. 169, 17–27. https://doi.org/10.1144/0016-76492010-186.
Lemirre, B., Cochelin, B., Duchene, S., de Saint Blanquat, M., Poujol, M., 2019. Origin and duration of late orogenic magmatism in the foreland of the Variscan belt (Lesponne — Chiroulet — Neouvielle area, French Pyrenees). Lithos 336–337, 183–201. https://doi.org/10.1016/j.lithos.2019.03.037.
Liesa, M., 1988. El metamorfisme del vessant sud del Massís del Roc de Frausa (Pirineus Orientals). PhD Thesis. Universitat de Barcelona, Unpublished, Barcelona, p. 288pp.
Liesa, M., Casas, J.M., Castiñeiras, P., Navidad, M., Carreras, J., 2008. Correlation of late neoproterozoic sequences of the eastern Pyrenees based on U-Pb (SHRIMP) zircon data. Geotemas 701–704.
Llorens, M.-G., Bons, P.D., Griera, A., Gomez-Rivas, E., 2013. When do folds unfold during progressive shear? Geology 41, 563–566. https://doi.org/10.1130/G33973.1.
Losantos, M., Palau, J., Carreras, J., Druguet, E., Santanach, P., Cirés, J., 1997. Mapa Geològic de Catalunya a escala 1:25.000. Institut Cartogràfic i Geològic de Catalunya. Hoja 259-1-1(79-21)-Roses.
Martí, J., Solari, L., Casas, J.M., Chichorro, M., 2019. New late Middle to early Late Ordovician U–Pb zircon ages of extension-related felsic volcanic rocks in the Eastern Pyrenees (NE Iberia): tectonic implications. Geol. Mag. 156, 1783–1792. https://doi.org/10.1017/S0016756819000116.
Martínez, F.J., Dietsch, C., Aleinikoff, J., Cirés, J., Arboleya, M.L., Reche, J., Gómez-Gras, D., 2016. Provenance, age, and tectonic evolution of Variscan flysch, southeastern France and northeastern Spain, based on zircon geochronology. Geol. Soc. Am. Bull. 128, 842–859. https://doi.org/10.1130/B31316.1.
Mauldon, M., Dunne, W.M., Rohrbaugh, M.B., 2001. Circular scanlines and circular windows: new tools for characterizing the geometry of fracture traces. J. Struct. Geol. 23, 247–258. https://doi.org/10.1016/S0191-8141(00)00094-8.
McCaig, A.M., Wickham, S.M., Taylor, H.P., 1990. Deep fluid circulation in alpine shear zones, Pyrenees, France: field and oxygen isotope studies. Contrib. Mineral. Petrol. 106, 41–60. https://doi.org/10.1007/BF00306407.
Miró, J., Muñoz, J.A., Manatschal, G., Roca, E., 2020. The Basque – Cantabrian Pyrenees: report of data analysis. In: Lacombe, O., Tavani, S., Teixell, A., Pedreira, D., Calassou, S. (Eds.), BSGF - Earth Sciences Bulletin 191, 22. https://doi.org/10.1051/bsgf/2020024.
Mondal, T.K., Mamtani, M.A., 2013. 3-D Mohr circle construction using vein orientation data from Gadag (southern India) – implications to recognize fluid pressure fluctuation. J. Struct. Geol. 56, 45–56. https://doi.org/10.1016/j.jsg.2013.08.005.
Müller, A., Herrington, R., Armstrong, R., Seltmann, R., Kirwin, D.J., Stenina, N.G., Kronz, A., 2010. Trace elements and cathodoluminescence of quartz in stockwork veins of Mongolian porphyry-style deposits. Miner. Deposita 45, 707–727. https://doi.org/10.1007/s00126-010-0302-y.
Muñoz, J.A., 2002. The Pyrenees. In: Gibbons, W., Moreno, T. (Eds.), The Geology of Spain. Geological Society London, London, pp. 370–385.
Muñoz, J.A., 1992. Evolution of a continental collision belt: ECORS-Pyrenees crustal balanced cross-section. In: McClay, K.R. (Ed.), Thrust Tectonics. Springer Netherlands, Dordrecht, pp. 235–246. https://doi.org/10.1007/978-94-011-3066-0_21.
Muñoz, J.-A., Beamud, E., Fernández, O., Arbués, P., Dinarès-Turell, J., Poblet, J., 2013. The Ainsa Fold and thrust oblique zone of the central Pyrenees: kinematics of a curved contractional system from paleomagnetic and structural data: paleomagnetism in S pyrenees. Tectonics 32, 1142–1175. https://doi.org/10.1002/tect.20070.
Muñoz, J.A., Mencos, J., Roca, E., Carrera, N., Gratacós, O., Ferrer, O., Fernández, O., 2018. The structure of the South-Central-Pyrenean fold and thrust belt as constrained by subsurface data. Geol. Acta 22.
Nabavi, S.T., Fossen, H., 2021. Fold geometry and folding – a review. Earth Sci. Rev. 222, 103812 https://doi.org/10.1016/j.earscirev.2021.103812.
Navidad, M., Castiñeiras, P., Casas, J.M., Liesa, M., Belousova, E., Proenza, J., Aiglsperger, T., 2018. Ordovician magmatism in the eastern Pyrenees: implications for the geodynamic evolution of northern Gondwana. Lithos 314–315, 479–496. https://doi.org/10.1016/j.lithos.2018.06.019.
Oriolo, S., Wemmer, K., Oyhantçabal, P., Fossen, H., Schulz, B., Siegesmund, S., 2018. Geochronology of shear zones – a review. Earth Sci. Rev. 185, 665–683. https://doi.org/10.1016/j.earscirev.2018.07.007.
Ortiz, A., Perconig, E., 1975. Memoria asociada al mapa de la hoja 61 (Bilbao) del Mapa Geológico de España. Instituto Geológico y Minero de España (IGME) - Serie MAGNA50.
Padel, M., Álvaro, J.J., Casas, J.M., Clausen, S., Poujol, M., Sánchez-García, T., 2018a. Cadomian volcanosedimentary complexes across the Ediacaran–cambrian transition of the eastern Pyrenees, southwestern Europe. Int. J. Earth Sci. 107, 1579–1601. https://doi.org/10.1007/s00531-017-1559-5.
Padel, M., Clausen, S., Álvaro, J.J., Casas, J.M., 2018b. Review of the Ediacaran-lower ordovician (pre-Sardic) stratigraphic framework of the eastern Pyrenees, southwestern Europe. Geol. Acta 16, 339–365.
Pavelsky, T.M., Smith, L.C., 2008. RivWidth: a software tool for the calculation of river widths from remotely sensed imagery. Geosci. Rem. Sens. Lett. IEEE 5, 70–73. https://doi.org/10.1109/LGRS.2007.908305.
Peacock, D.C.P., Sanderson, D.J., Bastesen, E., Rotevatn, A., Storstein, T.H., 2019. Causes of bias and uncertainty in fracture network analysis. Norw. J. Geol. https://doi.org/10.17850/njg99-1-06.
Pereira, M.F., Castro, A., Chichorro, M., Fernández, C., Díaz-Alvarado, J., Martí, J., Rodríguez, C., 2014. Chronological link between deep-seated processes in magma chambers and eruptions: Permo-Carboniferous magmatism in the core of Pangaea (Southern Pyrenees). Gondwana Res. 25, 290–308. https://doi.org/10.1016/j.gr.2013.03.009.
Poitrenaud, T., Poujol, M., Augier, R., Marcoux, E., 2020. The polyphase evolution of a late Variscan W/Au deposit (Salau, French Pyrenees): insights from REE and U/Pb LA-ICP-MS analyses. Miner. Deposita 22.
Santanach, P., 1972a. Estudio tectónico del Paleozoico inferior del Pirineo entre la Cerdaña y el río Ter. Acta Geol. Hisp. 7, 44–49.
Santanach, P., 1972b. Sobre una discordancia en el Paleozoico inferior de los Pirineos orientales. Acta Geol. Hisp. 7, 129–132.
Santolaria, P., Casas-Sainz, A.M., Soto, R., Casas, A., 2017. Gravity modelling to assess salt tectonics in the western end of the South Pyrenean Central Unit. J. Geol. Soc. 174, 269–288. https://doi.org/10.1144/jgs2016-027.
Sharp, Z.D., Masson, H., Lucchini, R., 2005. Stable isotope geochemistry and formation mechanisms of quartz veins; extreme paleoaltitudes of the Central Alps in the Neogene. Am. J. Sci. 305, 187–219. https://doi.org/10.2475/ajs.305.3.187.
Sillitoe, R.H., 2010. Porphyry copper systems. Econ. Geol. 105, 3–41. https://doi.org/10.2113/gsecongeo.105.1.3.
Stall, S., Yarmey, L., Cutcher-Gershenfeld, J., Hanson, B., Lehnert, K., Nosek, B., Parsons, M., Robinson, E., Wyborn, L., 2019. Make scientific data FAIR. Nature 570, 27–29. https://doi.org/10.1038/d41586-019-01720-7.
Tannock, L., Herwegh, M., Berger, A., Liu, J., Lanari, P., Regenauer-Lieb, K., 2020. Microstructural analyses of a giant quartz reef in south China reveal episodic brittle-ductile fluid transfer. J. Struct. Geol. 130, 103911 https://doi.org/10.1016/j.jsg.2019.103911.
Tannock, L., Herwegh, M., Berger, A., Regenauer-Lieb, K., 2019. The mineral factory: how to build a giant quartz reef. ASEG Extended Abstracts 1–4. https://doi.org/10.1080/22020586.2019.12072994, 2019.

Thiele, S.T., Grose, L., Samsu, A., Micklethwaite, S., Vollgger, S.A., Cruden, A.R., 2017. Rapid, semi-automatic fracture and contact mapping for point clouds, images and geophysical data. Solid Earth 13.

Tugend, J., Manatschal, G., Kusznir, N.J., 2015. Spatial and temporal evolution of hyperextended rift systems: implication for the nature, kinematics, and timing of the Iberian-European plate boundary. Geology 43, 15–18. https://doi.org/10.1130/G36072.1.

Vacherat, A., Mouthereau, F., Pik, R., Huyghe, D., Paquette, J.-L., Christophoul, F., Loget, N., Tibari, B., 2017. Rift-to-collision sediment routing in the Pyrenees: a synthesis from sedimentological, geochronological and kinematic constraints. Earth Sci. Rev. 172, 43–74. https://doi.org/10.1016/j.earscirev.2017.07.004.

Vissers, R.L.M., van Hinsbergen, D.J.J., Wilkinson, C.M., Ganerød, M., 2017. Middle jurassic shear zones at Cap de Creus (eastern Pyrenees, Spain): a record of pre-drift extension of the Piemonte–Ligurian ocean? J. Geol. Soc. 174, 289–300. https://doi.org/10.1144/jgs2016-014.

Wangen, M., Munz, I.A., 2004. Formation of quartz veins by local dissolution and transport of silica. Chem. Geol. 14.

Weisheit, A., Bons, P.D., Danišík, M., Elburg, M.A., 2013a. Crustal-scale folding: palaeozoic deformation of the Mt painter inlier, south Australia. Geological Society, London, Special Publications 394, 53–77. https://doi.org/10.1144/SP394.9.

Weisheit, Anett, Bons, P.D., Elburg, M.A., 2013b. Long-lived crustal-scale fluid flow: the hydrothermal mega-breccia of Hidden Valley, Mt. Painter Inlier, South Australia. Int. J. Earth Sci. 102, 1219–1236. https://doi.org/10.1007/s00531-013-0875-7.

Wilkinson, M.D., Dumontier, M., Aalbersberg, IjJ., Appleton, G., Axton, M., Baak, A., Blomberg, N., Boiten, J.-W., da Silva Santos, L.B., Bourne, P.E., Bouwman, J., Brookes, A.J., Clark, T., Crosas, M., Dillo, I., Dumon, O., Edmunds, S., Evelo, C.T., Finkers, R., Gonzalez-Beltran, A., Gray, A.J.G., Groth, P., Goble, C., Grethe, J.S., Heringa, J., 't Hoen, P.A.C., Hooft, R., Kuhn, T., Kok, R., Kok, J., Lusher, S.J., Martone, M.E., Mons, A., Packer, A.L., Persson, B., Rocca-Serra, P., Roos, M., van Schaik, R., Sansone, S.-A., Schultes, E., Sengstag, T., Slater, T., Strawn, G., Swertz, M. A., Thompson, M., van der Lei, J., van Mulligen, E., Velterop, J., Waagmeester, A., Wittenburg, P., Wolstencroft, K., Zhao, J., Mons, B., 2016. The FAIR Guiding Principles for scientific data management and stewardship. Sci. Data 3, 160018. https://doi.org/10.1038/sdata.2016.18.

Yardley, B.W.D., Banks, D.A., Bottrell, S.H., Diamond, L.W., 1993. Post-metamorphic gold-quartz veins from N.W. Italy: the composition and origin of the ore fluid. Mineral. Mag. 57, 407–422. https://doi.org/10.1180/minmag.1993.057.388.05.

Zhang, L., Groves, D.I., Yang, L.-Q., Sun, S.-C., Weinberg, R.F., Wang, J.-Y., Wu, S.-G., Gao, L., Yuan, L.-L., Li, R.-H., 2020. Utilization of pre-existing competent and barren quartz veins as hosts to later orogenic gold ores at Huangjindong gold deposit, Jiangnan Orogen, southern China. Miner. Deposita 55, 363–380. https://doi.org/10.1007/s00126-019-00904-5.

Zwart, H.J., 1986. The variscan geology of the Pyrenees. Tectonophysics 129, 9–27. https://doi.org/10.1016/0040-1951(86)90243-X.